4

Nonlinear Response of the Static and Dynamic Phases of the Vortex Matter

S. S. Banerjee[1], Shyam Mohan[1], Jaivardhan Sinha[1],
Yuri Myasoedov[3], S. Ramakrishnan[2] and A. K. Grover[2]
[1]*Department of Physics, Indian Institute of Technology Kanpur, Uttar Pradesh*
[2]*Department of Condensed Matter Physics and Materials Science,*
Tata Institute of Fundamental Research, Mumbai,
[3]*Department of Physics, Weizmann Institute of Science, Rehovot,*
[1,2]*India*
[3]*Israel*

1. Introduction

In the mixed state of type II superconductors, the external magnetic field penetrates the superconducting material in the form of normal cored regions, each carrying a quantum of flux ($\Phi_0 = 2.07\times10^{-7}$ G-cm^2). These normal cores have radii equal to the coherence length (ξ). Surrounding each normal core is a vortex of supercurrent that decays over a characteristic length scale known as the penetration depth (λ). These elastic string-like normal entities (or vortices) mutually repel each other leading to the formation of triangular vortex lattices in ideal superconductors (Blatter et al., 1994; Natterman & Scheidl, 2000). However, real samples always have defects (point defects, dislocations) and inhomogeneities. The superconducting order parameter is preferentially suppressed at these random defect locations, thereby energetically favoring pinning of vortices at these locations. But, pinning also leads to loss of long range order in the vortex lattice. The vortex matter can be considered as a typical prototype for soft materials, where pinning forces and thermal fluctuations are comparable to the elastic energy scale of the vortex lattice. The perennial competition between elastic interactions in the vortex lattice, which establishes order in the vortex state and effects of pinning and thermal fluctuations which try to destabilize the vortex lattice, leads to a variety of pinning regimes, viz., the weak collective pinning regime and the strong pinning regime (Blatter et al., 2004). The competition in different portions of the field-temperature (H,T) phase space leads to the emergence of a variety of vortex phases, like, the Bragg glass, vortex glass, vortex liquid (for review see, Blatter et al., 1994; Natterman & Scheidl, 2000) and transformation amongst them, along with the appearance of significant thermomagnetic history dependent response. The competing effects ever present in the vortex lattice also lead to a quintessential phenomenon called the peak effect (PE), which we shall discuss in the next section.

2. The peak effect phenomenon

Theoretical works in late nineteen eighties and nineties have shown that by taking into account the effects of thermal fluctuations and pinning centers on vortices, the mean field description of a type II superconductor gets substantially modified and new phases and phase boundaries in the vortex matter were predicted. In particular, in a clean pinning free system, it was shown that under the influence of thermal fluctuations, the vortex lattice phase is stable only in the intermediate field range. A new phase was predicted to be present at both very low and at very high fields, viz., the Vortex Liquid State (Nelson, 1988), in which the r.m.s, fluctuation of the vortices about their mean positions become ~10 – 20 % of the intervortex spacing a_0 ($a_0 \propto B^{1/2}$, where B is the field) and the vortex-vortex spatial correlations reduced down length scales of the order ~ a_0. Experimental works on the high temperature superconductors (HTSC) have established the vortex solid to liquid transition at high fields, however, the demonstration of the reentrant behavior of the vortex solid to liquid phase boundary has so far not been vividly elucidated (Blatter et al, 1998; Natterman & Scheidl, 2000). The mean field picture of a perfectly periodic arrangement of vortices in the vortex solid phase is also expected to be modified under the influence of pinning and the vortex solid phase is considered to behave like a vortex glass (Fisher 1989; Fisher, et al. 1989), which is characterized by zero linear resistivity, and could exhibit many metastable states. Further detailed investigations (Giammarchi and P. Le Doussal, 1995), showed, the existence of a novel vortex solid to solid transformation as a function of varying field at a fixed temperature in which a novel Bragg Glass phase (a reasonably well ordered lattice with correlation extending over few hundreds of a_0) at low fields transforms into a Vortex Glass state with spatial correlations surviving over a very short range at high fields. This solid to solid transformation is considered to arise due to a sudden injection / proliferation of dislocations into the Bragg glass phase (for a review see Natterman & Scheidl, 2000).

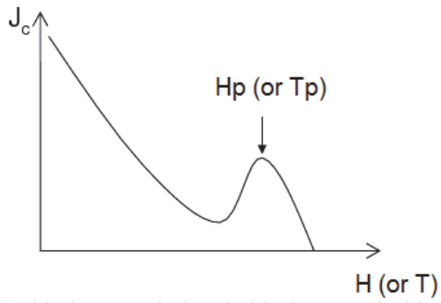

Fig. 1. Schematic representation of the peak effect (PE) in the critical current density, J_c, with applied field (or temperature). The field H_p (or temperature T_p) represents the peak position of the PE.

To experimentally investigate the phases of vortex matter, few popular routes are via ac susceptibility, dc magnetization, transport measurements, all of which provide information on the critical current density (J_c) (the maximum dissipationless current which is carried by a superconductor). Usually a change in the phase of vortex matter is accompanied by a change in the pinning experienced by the vortices. As the J_c is a direct measure of the pinning experienced by a given phase, changes in the behavior of J_c are a good indicator of the transformation/transition in the vortex matter. Usually the J_c of a superconductor is expected to monotonically decrease with increasing values of the temperature or field. However, in a large variety of superconductors it is found that the monotonic decrease in J_c

with increasing field (H) or temperature (T) is interrupted by an anomalous enhancement in J_c just before the superconductor turns normal (Figure.1). This anomaly in the J_c behavior is known as the peak effect (PE) phenomenon and has been observed in many low and high-temperature superconductors (Berlincourt, 1961; Bhattacharya & Higgins, 1993; Higgins and Bhattacharya, 1996; Ling et al., 2001; Ghosh et al., 1996; Banerjee et al., 1998, 1999a, 1999b, 2000a, 2000b, 2001). In electrical transport experiments, from which J_c is deduced, the PE appears as a bump in J_c as in the schematic of Fig.1. Due to the enhancement in pinning, the PE appears as an anomalous increase of the diamagnetic screening or shielding response and a drop in the dissipation response in the ac susceptibility (quadrature signal) measurements before the diamagnetic ac-susceptibility (in -phase signal) crashes to zero at H_{c2} or $T_c(H)$ (Banerjee et al., 1998-2001; Mohan et al., 2007).

Though a complete theoretical description of the PE is lacking, there have been plausible proposals articulating different mechanisms to explain this phenomenon. Pippard (Pippard, 1969) put forth the notion that if the vortex lattice (VL) loses rigidity near H_{c2} at a rate much faster than the pinning force, then the softened vortices would conform more easily to the pinning centers thereby getting strongly pinned, and consequently producing the peak in J_c. The idea acquired a quantitative basis, when a correct statistical summation procedure for the pinning force was proposed by A. I. Larkin and Yu. N. Ovchinnikov (LO) (Larkin, 1970a, 1970b; Larkin and Ovchinnikov, 1979), which took into account the elasticity of the vortex lattice. The basic premise of the LO theory is that the flux lines lower their free energy by passing through the pinning sites, thereby deviating from an ideal periodic arrangement. The deformation of the FLL costs elastic energy despite the lowering in free energy due to the pinning of flux lines. The equilibrium configuration of the flux lines in a deformed state is obtained by minimizing the sum of these two energies. This work of Larkin and Ovchinnikov showed that random distribution of weak pins destroys long range order in the FLL, with short range order being preserved only within a volume bounded by two correlation lengths viz., the radial (R_c, the correlation length across the surface of the sample and perpendicular to the vortex line) and the longitudinal (L_c, the correlation length parallel to the vortex line). These length scales were shown to be related to the elastic modulii of the vortex lattice (Larkin and Ovchinnikov, 1979), and the net pinning force experienced by the VL, viz., $F_p \propto R_c^{-\alpha} L_c^{-\beta}$, where α and β are positive powers. The PE stood explained within the LO theory due to softening of the elastic modulii of the VL, which caused a decrease in R_c and L_c, thereby causing F_p or J_c to anomalously increase at PE. While the LO theory provides an explanation of the PE phenomenon, a quantitative match of the details of the PE with LO theory lacked.

While theoretically some difference persist as regards the origin of the PE phenomenon, the experimental investigations (Banerjee et al., 1998, 1999a, 1999b, 2000a, 2000b, 2001; Bhattacharya & Higgins, 1993; Gammel et al., 1998; Ghosh et al, 1996; Higgins and Bhattacharya, 1996; Marchevsky et al., 2001; Thakur et. al, 2005, 2006; Troyanovski et al., 1999, 2002) are almost concurrent towards in establishing PE as an order to disorder transformation in the vortex lattice. Studies (Banerjee et al, 1998, 1999a, 1999b, 2000a,b, 2001) on different single crystals of 2H-$NbSe_2$, with progressively increasing amounts of the quenched random pinning have revealed that the details of PE phenomenon are significantly affected by level of disorder, amounting to the appearance of significant variation in the metastable response(s) of the vortex lattice. These studies were able to demonstrate the correlation between the thermomagnetic history effects (i.e., difference

between the field cooled (FC) and zero - field cooled (ZFC) response exhibited by the FLL in single crystal of a conventional superconductor 2H-$NbSe_2$ and the pinning strength in the samples (Banerjee et al, 1999b). These observations lead to proposals pertaining to the existence of a pinning induced transformation across glassy phases of the vortex matter. In recent times an interesting explanation for PE has been proposed based on a crossover from weak to collective pinning in the vortex matter (Blatter et al. 2004). We shall discuss this work in relation to the experimental findings in section 3.3.

2.1 The effect of disorder on the behavior of critical current (J_c) and the peak effect (PE) phenomenon

2.1.1 Single crystals of different pinning strengths

We are collating here results reported on good quality single crystals of 2H-$NbSe_2$, grown in different laboratories (University of Warwick, UK, NEC research Institute, Princeton, USA and Bell Labs, Murray Hills, USA). On the basis of correlation between pinning strength and the metastability effects in the elastic region of vortex phase diagram, the crystals can be sequentially enumerated in terms of the progressively enhanced pinning. For instance, in 2H-$NbSe_2$ crystals, ranging from nomenclature A to C, the J_c values vary from 10 A/cm² to 1000 A/cm² (Banerjee et al., 1998, 1999a, 1999b, 2000a, 2000b, 2001; Thakur et al. 2005, 2006).

2.1.2 Identification of different pinning regimes and the behavior of PE as a function of pinning

We extracted $J_c(H)$ (for H//c) in two varieties of single crystals A and B, of 2H-$NbSe_2$, either by directly relating $J_c(H)$ to the widths of the isothermal magnetization hysteresis loops (Bean, 1962, 1964) or by analyzing the in-phase and out-of-phase ac susceptibility data (Bean, 1962, 1964; Angurel et al., 1997). Figure 2 summarizes the J_c vs. H data (H\\c) for the crystals A and B in two sets of log-log plots in the temperature regions close to the respective $T_c(0)$ values (Banerjee, 2000b; Banerjee et al. 2001). The peaks in $J_c(H)$ occur at fields (H_p) less than 1 kOe (see insets in Fig.2(c) and Fig.2(g) for the $t_p(H)$ curves in A and B, viz., locus of the PE in the H - reduced temperature ($t = T/T_c(0)$) space for the two samples, with pinning strength in B > A).

We first focus on the shapes of the $J_c(H)$ curves (cf. Fig.2(a) to 2(d)) in the crystal A. In Fig.2(a), the three regimes (marked I, II and III in the figure) of $J_c(H)$, at a reduced temperature t~0.973, are summarized as follows : (1) At the lowest fields ($H \leq 10$ Oe), J_c varies weakly with H (region I), as expected in the individual pinning or small bundle pinning regime, noted earlier (Duarte et al. 1996), (2) Above a threshold field value, marked by an arrow, $J_c(H)$ variation (in region II) closely follows the archetypal collective pinning power law (Duarte et al. 1996, Larkin, 1970a, 1970b; Larkin and Ovchinnikov, 1979) dependence (see the linear behaviour in region II of J_c vs. H on log-log scale in Fig.2), (3) This power law regime terminates at the onset (marked by another arrow) position of the PE phenomenon (region III).

On increasing the temperature (see Figs. 2(a) and 2(b) for the data at t=0.973 and 0.994), the following trends are immediately apparent: (1) the peak effect becomes progressively shallower, i.e., the ratio of $J_c(H)$ at the peak position to that at the onset of PE becomes smaller. For instance, the said ratio has a value of about 8 at t=0.973 and it reduces to a value of 3.5 at t=0.994. ; (2) The power law region shrinks; for example, the field interval between the pair of arrows (identifying the power law region) spans from 10 Oe to about 500 Oe at

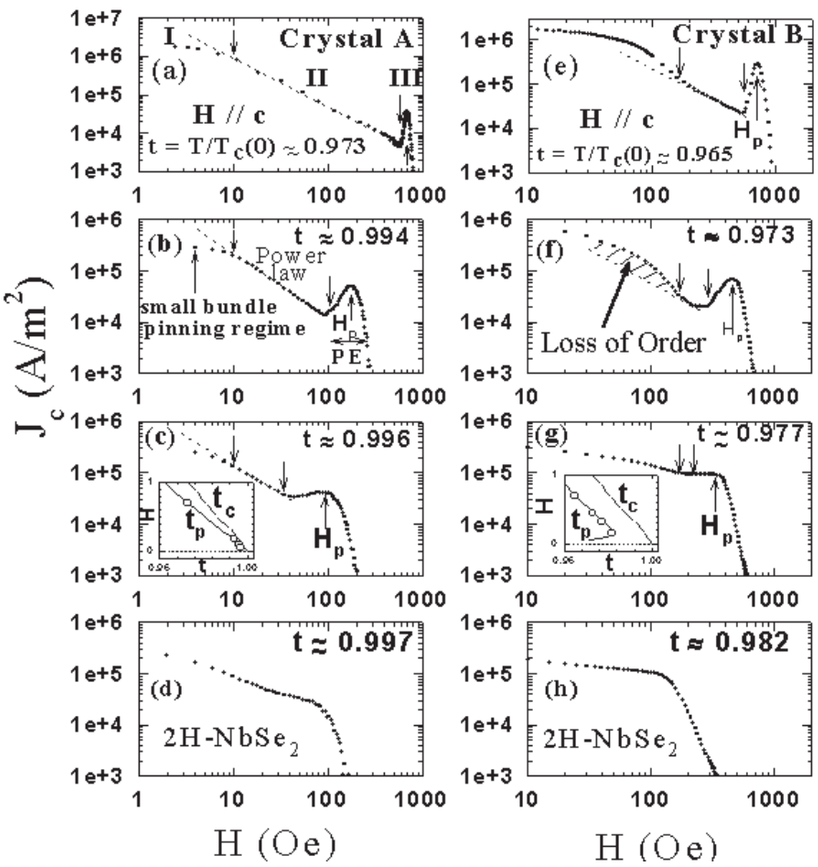

Fig. 2. Log-Log plots of J_c vs. H for H\\c at selected reduced temperatures ($t = T/T_c(0)$) in crystals A and B of 2H- $NbSe_2$. The insets in Fig.2(c) and Fig.2(g) display the locus of PE curve, $t_p(H)(=T_p(H)/T_c(0))$ and the superconductor-normal phase boundary $t_c(H)(=T_c(H)/Tc(0))$ in crystals A and B, respectively. The marked data points on the PE curves in each of these insets identify the reduced temperatures at which $J_c(H)$ data have been displayed in Figs.2(a) to 2(d) and in Figs.2(e) to 2(h). (Ref. Banerjee et al, 2000a)

t=0.973 in Fig.2(a), whereas at t=0.996 in Fig. 2(c), the power law regime terminates near 40 Oe. Also, the slope value of linear variation of log J_c vs. log H in the latter case is somewhat smaller. At still higher temperatures (see, for instance, Fig.2(d) at 0.997), the power law region is nearly invisible and the anomalous PE peak cannot be distinctly identified anymore, as only a residual shoulder survives.

In contrast, the second set of plots (see Figs. 2(e) to 2(h)) in the crystal B shows a different behaviour, although the overall evolution in the shapes of $J_c(H)$ curves is generically the same. In Fig.2(e), at a reduced temperature t~0.965, one can see the same power law regime as in Fig.2(a), but as the extrapolated dotted line shows, $J_c(H)$ departs from the power law behaviour in the low field region (i.e., for H < 200 Oe). As the field decreases below 200 Oe, the current density in crystal B (t=0.965) increases rapidly towards the background saturation limit (i.e., in the single vortex pinning regime). The approach to background saturation limit occurs at much lower field (H < 10 Oe) in crystal A. The smooth crossover to individual or small bundle pinning regime as seen in the crystal A, therefore adds on an additional characteristic in the crystal B. We label the region of rapid rise of $J_c(H)$ at low

fields from a power law behaviour in region II into the weakly field dependent $J_c(H)$ behaviour in region I, as the region with "loss of order" (cf. Fig.2(f)). Further, with increasing temperature, the power law regime in the crystal B shrinks faster than that in sample A (cf. Fig.2(e) at t=0.965 and Fig.2(f) at t=0.973), leaving only a rather featureless monotonic $J_c(H)$ behaviour upto the highest fields (cf. Fig.2(g) and Fig.2(h)). Note, also, that the limiting value of the reduced temperature upto which the power law regime along with the PE peak survives in the crystal B is smaller than that in crystal A. In crystal B, the PE peak can be distinctly discerned only upto t=0.977, whereas in crystal A it can be seen even upto t=0.994. Recalling that the crystal B is more strongly pinned than crystal A, the above observation reaffirms the notion that the progressive enhancement in effective pinning (which occurs as we go from sample A to B) shrinks the (H,T) region over which the vortex matter responds like an elastically (ordered) pinned vortex lattice.

Having identified the regime of collective pinning where the vortex matter behaves like an ordered elastic medium and determined its sensitivity to pinning, it is fruitful to explore transformation in the elastic regime for weak collective to strong pinning (Blatter et al., 2004), and investigate if it coincides with the appearance of PE

3. Weak collective pinning, strong pinning and thermal fluctuations dominated regimes for the quasi-static vortex state

3.1.1 AC susceptibility measurements:

It is chosen to focus on A′ type of a crystal of 2H-$NbSe_2$ (cf. section 2.1.1, A′ has pinning inbetween that of samples A and B), has dimensions 1.5 x 1.5 x 0.1 mm^3, $T_c(0) \sim 7.2$ K and $J_c \sim 50 - 100$ A/cm^2 (at 4.2 K and 10 kOe). The 2H-$NbSe_2$ system, being a layered material, often has extended defects (dislocations, stacking faults) present along its crystalline *c* axis. If H is applied along the *c* axis, then the vortex lines (also oriented along *c* direction) could be strongly pinned by these extended defects between layers. To reduce the emphasis on the inevitably present strong pinning centers, we have chosen to focus on behaviour obtained for the $H \perp c$ orientation (the c-axis of hexagonal crystallographic lattice is aligned along the thickness of the platelet shaped sample) for our measurements. This choice of the field direction also avoids geometric and surface barrier effects, which are known to persist up to the PE in H //c orientation (Zeldov, et al. 1994; Paltiel et al., 1998).

We measured the ac susceptibility response as well as DC magnetization of the vortex state in the weak pinning 2H-$NbSe_2$ sample in the above mentioned orientation. The real (χ') component of the ac susceptibility response (viz., $\chi=\chi'+i\chi''$) is a measure of its diamagnetic shielding response. The maximum value of (normalized) $\chi'= -1$ corresponds to the perfectly shielded, Meissner state of the superconductor. The χ' is related to the shielding currents (= J_c) setup in the sample via (Bean 1962, 1964), $\chi' \propto -J_c / h_{ac}$ for $h_{ac} > H^*$, where h_{ac} is the ac excitation magnetic field used to measure the ac susceptibility response and H^* is the penetration field value at which induced screening currents flow through the entire bulk of the sample. (Note, $H^* \propto J_c(H,T)$). The quadrature χ'' signal is a measure of energy dissipated by vortices, which maximizes at $h_{ac} = H^*$. If the vortices get strongly pinned then χ''shows a decrease, which is encountered in the PE regime. In the PE region, vortex matter gets better pinned and the χ'' response anomalously decreases.

3.1.2 Typical characteristics of AC susceptibility response

The $\chi'(T)$ behavior in the presence of a dc field (H) of 100 Oe is shown in Fig.3(a). In this figure the various curves correspond to different values of the amplitude of the h_{ac} at a frequency of 211 Hz applied parallel to H ($\perp$ c). Note that at a fixed T, on increasing h_{ac} the χ' (viz., the diamagnetic shielding) response progressively decreases from -1 value (see the dashed arrow marked at 6.8 K in Fig.3(a)). At fixed T, the decrease in χ' is due to h_{ac} approaching close to H* ($\propto J_c$(100 Oe, 6.8 K) and the magnetic flux penetrates the bulk of the sample, leading to a decrease in the screening response. As the h_{ac} penetrates deeper into the superconductor, one begins to clearly observe features associated with the bulk pinning of vortices inside the superconductor, viz., the peak effect (PE) phenomenon. The quintessential PE is easily observed as the anomalous enhancement in χ' between T_{on} (corresponding to the onset of PE at a given H, T) and T_p (the peak of PE at a given H, T) . Notice that due to the enhanced pinning in the PE regime between T_{on} and T_p, the sample attempts to shield its interior better from the penetrating h_{ac} as a consequence the χ' increases. Also notice that as the h_{ac} increases, the PE width between T_{on} and T_p becomes narrower.

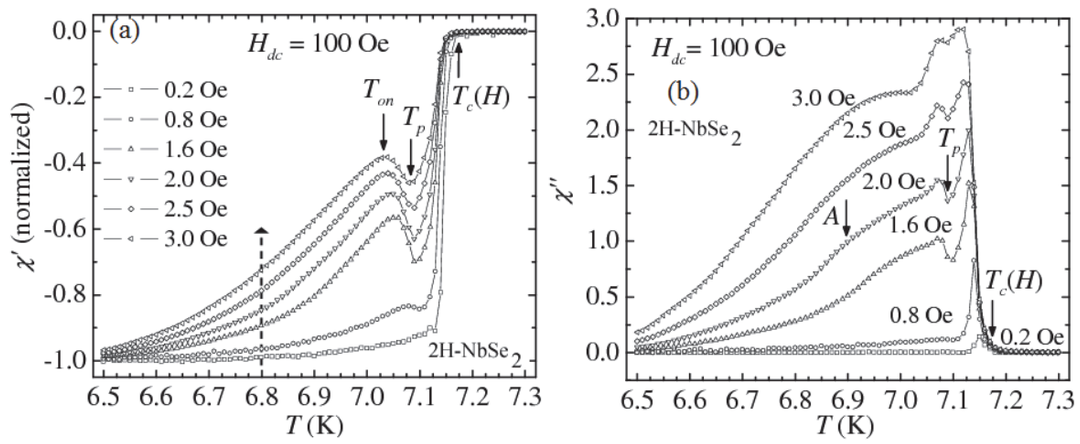

Fig. 3. (a) The behaviour of $\chi'(T)$ at H=100 Oe for different values of h_{ac}. T_{on} and T_p denote the onset and peak temperatures of the PE phenomenon. (b) The $\chi''(T)$ behaviour at H=100 Oe for different values of h_{ac}. Location marked as A indicates the broad dissipation peak due to penetration of h_{ac} into the bulk of the sample (h_{ac} > H*). [Banerjee 2000b; Mohan (2009)b]

The behaviour of the out-of-phase component (χ'') of the ac susceptibility for various values of h_{ac} at H =100 Oe is shown in Fig,.3(b). It is clear that for h_{ac} < 1 Oe and at low T, due to almost complete shielding of the probing h_{ac} from the bulk of the sample, the χ''response is nearly zero. At a fixed T, say T=6.8 K, as h_{ac} increases, χ'' response also increases monotonically. Full penetration of h_{ac} into the bulk of the sample causes a significant rise in dissipation, which in turn leads to a broad maximum in the χ'' response (location marked as A in Fig.3(b) for h_{ac} =2 Oe). On approaching the PE region, due to enhancement in vortex pinning, one observes a drop in χ''response (marked as T_p for h_{ac} = 2 Oe). Beyond T_p, dissipation has a tendency to rise sharply before decreasing close to T_c(H). From Fig.3(b) we note that at H =100 Oe and T=6.8 K, significant flux penetration starts at h_{ac} = 1.6 Oe. Within the Bean's Critical State model (Bean 1962, 1964) the field for flux penetration is given by H*~J_c.d, where d is the relevant dimension in which the critical state is established. Using Fig.3(b), by approximating H*= 1.6 Oe, we estimate the J_c ~ 130 A/cm^2 at 6.8 K at 100 Oe (note J_c decreases significantly with increasing H).

3.2 Transformation in the vortex state deep in the elastic regime

From Fig.3 it can be noted that the PE phenomenon is distinctly observed for $h_{ac} \geq 2$ Oe as at these h_{ac}, the ac field fully penetrate the bulk of the superconductor, and one can probe changes in the bulk pinning characteristics of the sample. Choosing $h_{ac} = 2$ Oe, we measured the $\chi'(T)$ and $\chi''(T)$ for different values of H. Figures 4(a) and 4(c) and Figs. 4(b) and 4(d)

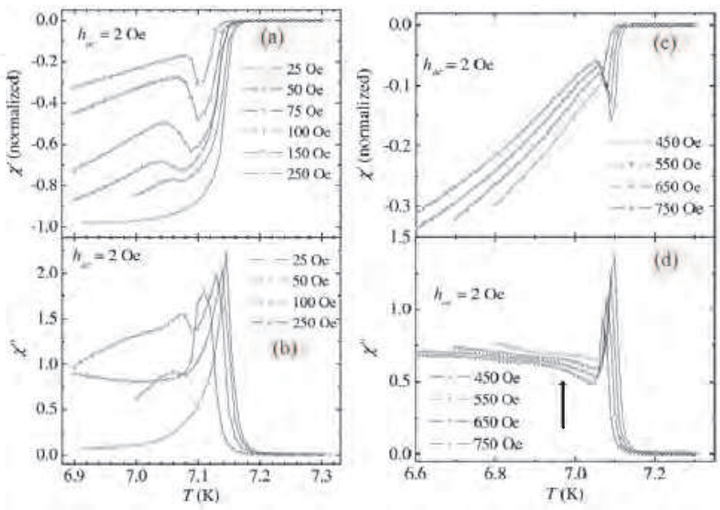

Fig. 4. The real ((a),(c)) and imaginary ((b), (d)) parts of the ac susceptibility as a function of T with h_{ac}=2 Oe and for different H. [Mohan 2009b]

show the $\chi'(T)$ and $\chi''(T)$, respectively. At 7.0 K in Fig.4(a), with increasing H the value of χ'varies from about -1 at 25 Oe to about -0.2 at 250 Oe. This decrease in the diamagnetic shielding response, we believe, arises from the inverse field relation of the critical current density, e.g., $J_c \propto 1/H$ (Kim et al., 1962). In all the curves the location of PE is clearly visible as the anomalous enhancement in χ' due to the anomalous increase in pinning or J_c. However below 100 G the PE is very shallow, and we see an enhancement in χ''which occurs very close to $T_c(H)$. At 100 Oe we see the decrease in χ'' at PE quite clearly, before the χ''increases near $T_c(T)$. At higher fields of 250 Oe (Fig.4(a)) from $\chi'(T)$ we see that the PE gets narrower in temperature width. As one moves to still higher fields (Fig.4(c)), the PE width gets still narrower and sharper. In the $\chi''(T)$ at Fig.4(d), as well as in Fig.4(b) (above 100 Oe) we do not find the drop in χ'' associated with PE as the drop over a narrow temperature window in χ'' due to PE gets merged into the enhancement in χ'' signal one observes in the vicinity of $T_c(H)$. However from Figs.4(c) and 4(d), we see that there is a decrease in χ'' which begins (see an arrow in Fig.4(d)) well before the anomalous enhancement in $\chi'(T)$ sets in at PE.

The fig. 5 provides a glimpse into ac susceptibility data at high fields. Above H = 750 Oe, the signature of PE survives as a subtle change in slope of $\chi'(T)$ at T_p (see locations marked by arrows in Fig.5(a)) just before χ'crashes to zero value at $T_c(H)$. A distinct feature seen at these fields is that the dissipation χ'' behaviour (Fig.5(b)), which is large at lower T, decreases sharply as one approaches T_c. This decrease begins from a region located far below the PE and is similar to the decrease in $\chi''(T)$ found above 450 Oe in fig. 4(d). The sharp increase in the dissipation (on $\chi''(T)$) very close to $T_c(H)$ (as noted in Fig.4), is observed only for 1000 Oe

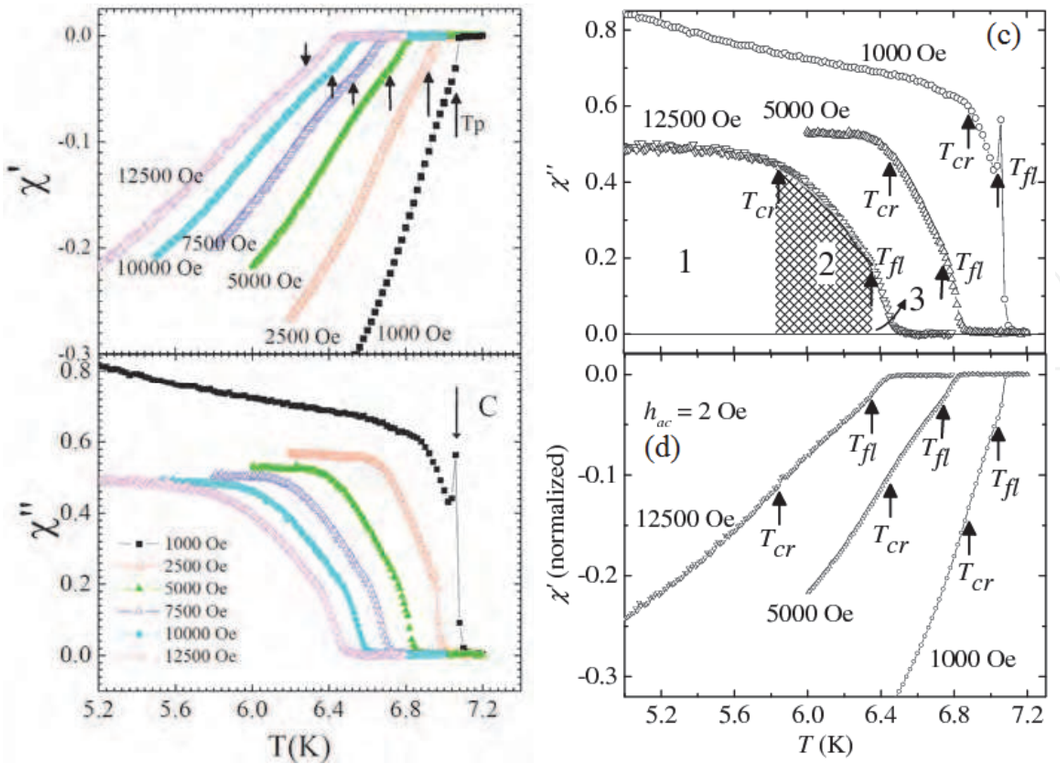

Fig. 5. The real (a) and imaginary (b) parts of the ac susceptibility measured with h_{ac} = 2 Oe and for different dc fields: 1000 Oe ≤ H ≤ 12500 Oe. The arrows in panel (a) mark the peak locations of the PE. (c) The χ'' response for 1000 Oe, 5000 Oe and 12500 Oe. The T_{cr} and T_{fl} locations determine the different regimes of dissipation marked as the regions 1, 2 and 3 (See text for details). (d) The χ' response corresponding to (c). [Mohan et al. 2007; Mohan 2009b].

(position marked C in Fig.5(b)). Above 1000 Oe, instead of a peak in χ''(T), the χ'' response exhibits only a change in slope near T_c(H) before becoming zero on reaching T_c(H). It should be noted that the temperature at which where the χ''response drops sharply from a large value does not correspond to any specific feature in χ'(T) and, also, occurs well before the onset of PE. In Figs.6 (a) to (c) we can identify locations of the drop in dissipation χ'' by detecting the change in slope of through plots dχ''/dT vs T (see Figs.6(f), 6(e) and 6(d)) .
In Figs.6(d)-(f), the onset of the drop in dissipation at lower T is marked with arrows as T_{cr} and the T at which there occurs a change in slope of the dissipation curves close to T_c(H) are marked as T_{fl}. (The nomenclature T_{cr} and T_{fl}, signify the temperature above which, there occur pinning crossover and thermal fluctuation dominated regimes, respectively). The dashed lines are a guide to the eye representing the base line behavior of the dχ''/dT. The onset of deviation in dχ''/dT from the baseline identifies T_{cr} (cf. Figs.6(d) – (f)). In Figs.6 (d)-(f) the base lines for different H have been artificially offset for clarity in the data representation. After the locations of T_{cr} and T_{fl} are identified from dχ''/dT (cf. Figs.6(d) – (f)), their positions are identified and marked on the corresponding χ''(T) curves (Figs.6(a)-(c)). We now consider three representative χ''(T) curves, namely the response for 1000 Oe, 5000 Oe and 12500 Oe in Fig.5(c) to understand the significance of the T_{cr} and T_{fl}.

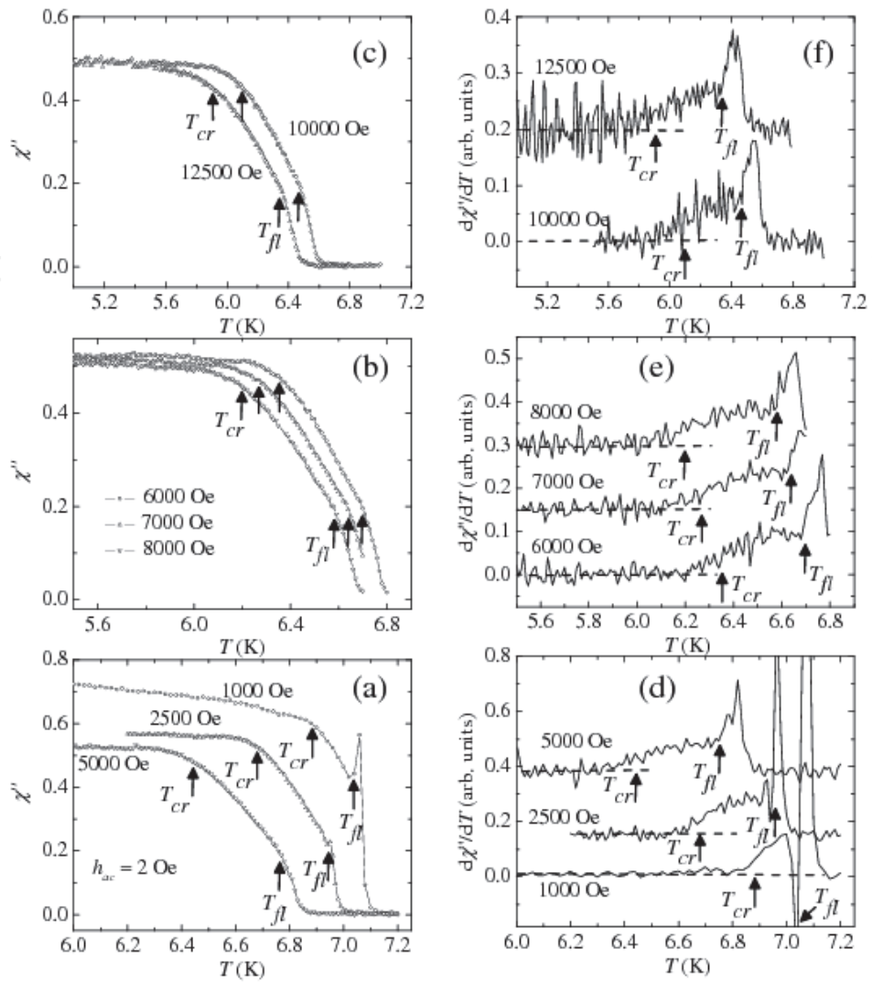

Fig. 6. The panels on the left (a)-(c) show the χ''(T) response for different H. The right hand panels (d)-(f), show the derivative dχ''/dT determined from the corresponding χ''(T) curves on the left panel. (see discussion in the text) [Mohan et al. 2007; Mohan 2009b]

In Fig.5(c), for H= 12500 Oe, three distinct regimes of behaviour in the χ''(T) response have been identified as the regions 1, 2 and 3. Region 1 is characterized by a high dissipation response. As noted earlier, this high dissipation results from full penetration of h_{ac} to the center of the sample, similar to the dissipation peak marked at A in Fig.3(b). As noted earlier in Fig.5(a), at these high fields beyond 1000 G, at T > T_{cr}, χ'(T) response possesses no distinct signature of the PE phenomenon. The absence of any distinct PE feature in χ'(T) should have caused no modulations in the behavior of χ''(T) response, except for a peak in dissipation close to T_c(H). Instead, in the region 2 (cross shaded and located between the T_{cr} and T_{fl} arrows in Fig.5(c)) a new behaviour in the dissipation response is observed, viz., in this region there is a substantial decrease in dissipation.

As seen earlier in the context of PE in Fig.3(b), that any anomalous increase in pinning corresponds to a decrease in the dissipation. The observation of a large drop in dissipation across T_{cr} (Fig.5(c)) indicates there is a transformation from low J_c state to a high J_c state, i.e., a transformation from weak pinning to strong pinning. Subsequent to the drop in χ''(T) in

region 2, the dissipation response attempts to show an abrupt increase (see change in slope in $d\chi''/dT$ in Fig.6(d) to (f)) at the onset of region 3 (marked as T_{fl} in Fig.5 and Fig.6). The abrupt increase in dissipation beyond T_{fl} is more pronounced at low H and high T (see behavior in Fig.5(b)). The significance of T_{fl} will be revealed in subsequent sections. In brief, the T_{fl} will be considered to identify the onset of a regime dominated by thermal fluctuations, where pinning effects become negligible and dissipation response goes through a peak. It is interesting to note that the T_{fl} locations are identical to the location of T_p (viz., the peak of PE) in Figs.5(a) and 5(c). For H < 750 Oe, the T_{fl} location can be identified with the appearance of a distinct PE peak at T_p (see Fig.4, where dissipation enhances at $T_p = T_{fl}$). It is important to reiterate that the anomalous drop in dissipation in region 2 near T_{cr} is not associated with the PE phenomenon.

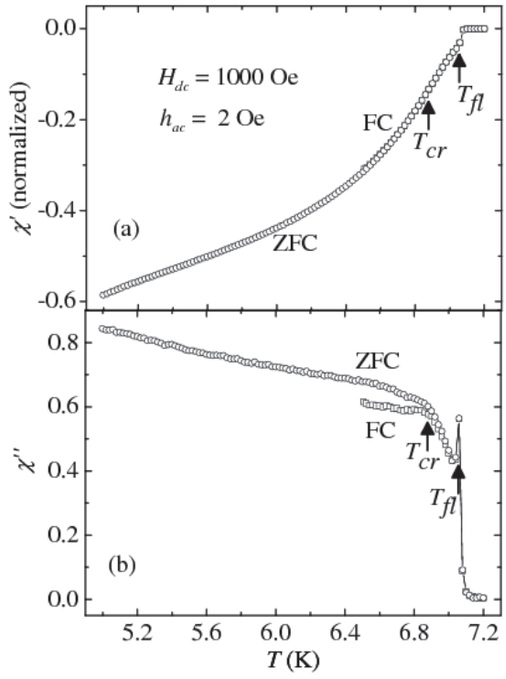

Fig. 7. The real (a) and imaginary (b) parts of the ac susceptibility measured in the ZFC and FC modes, for H = 1000 Oe. Also marked for are the locations of the T_{cr} and T_{fl}. [Mohan et al. 2007; Mohan 2009b]

All the above discussions pertain to susceptibility measurements performed in the zero field cooled (ZFC) mode. Detailed studies of the dependence of the thermomagnetic history dependent magnetization response on the pinning (Banerjee et al. 1999b, Thakur et al., 2006), had shown an enhancement in the history dependent magnetization response and enhanced metastablility developing in the vortex state as the pinning increases across the PE. While the ZFC and field cooling (FC), $\chi'(T)$ response can be identical in samples with weak pinning, the will show that $\chi''(T)$ is a more sensitive measure of small difference in the thermomagnetic history dependent response. Figures 7(a) and 7(b) display $\chi'(T)$ and $\chi''(T)$ measured for a vortex state prepared either in ZFC or FC state in 1000 Oe. Figure 7(a) shows the absence of PE at T_{cr} in the $\chi'(T)$ response at 1000 Oe for vortex state prepared in both FC and ZFC modes. Furthermore, there is no difference between the ZFC and FC $\chi'(T)$

responses (cf.Fig.7(a)). However, the dissipation ($\chi''(T)$) behaviour in the two states (Fig.7(b)) are slightly different. While there are no clear signatures of T_{cr} in the $\chi'(T)$ response, in $\chi''(T)$ response (Fig.7(b)) below T_{cr} one observes that the FC response significantly differs from that of the ZFC state, with the dissipation in the FC state below T_{cr} being lower as compared to that in the ZFC state. The presence of a strong pinning vortex state above T_{cr}, causes the freezing in of a metastable stronger pinned vortex state present above T_{cr}, when the sample is field cooled to $T < T_{cr}$. As the FC state has higher pinning than the ZFC state (which is in a weak pinning state) at the same T below T_{cr}, therefore, the $\chi''(T)$ response is lower for the FC state. Above T_{cr} the behavior of ZFC and FC curves are identical, as both transform into a maximally pinned vortex state above T_{cr}. The behavior of $\chi''(T)$ in the FC state indicates that the pinning enhances across T_{cr}. Beyond T_{cr}, the ZFC and FC curves match and the high pinning regime exists till T_{fl}. This observation holds true for all H_{dc} above 1000 Oe as well.

3.2.1 Transformation in pinning: evidence from DC magnetization measurements

Figure 8 displays measured forward (M_{fwd}) and (M_{rev}) reverse magnetization responses of 2H-$NbSe_2$ at temperatures of 4.4 K, 5.4 K and 6.3 K for $H \perp c$.

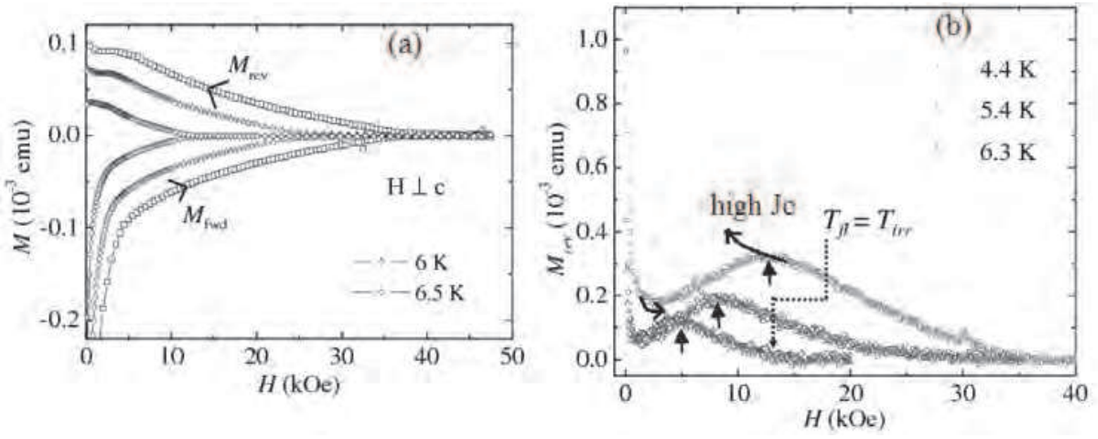

Fig. 8. The M-H hysteresis loops at different T. (a) The forward and reverse legs of the M-H loops are indicated as M_{fwd} and M_{rev}. (b) in M_{rev} (H) array at different T. The locations of the observed humps in the M_{rev}(H) curves are marked with arrows. Also indicated, in the 6.3 K curve, is the location of the field that corresponds to the temperature, $T_{fl} = T_{irr}$. [Mohan et al. 2007; Mohan 2009b]

A striking feature of the M-H loops in Fig. 8 is the asymmetry in the forward (M_{fwd}) and reverse (M_{rev}) legs. The M_{rev} leg of the hysteresis curve exhibits a change in curvature at low fields. In Fig.8(b) we plot only the M_{rev} from the M-H recorded at 4.4 K, 5.4 K and 6.3 K. At low fields, the M_{rev} leg exhibits a hump; the location of the humps are denoted by arrows in Fig.8(b). The characteristic hump-like feature (marked with arrows in Fig.8(b)) can be identified closely with T_{cr} locations identified in Figs.4, 5 and 6. The tendency of the dissipation χ'' to rapidly rise close to $T_{fl}(H)$ (cf. Figs.4, 5 and 6) is a behaviour which is expected across the irreversibility line ($T_{irr}(H)$) in the H-T phase diagram, where the bulk pinning and, hence, the hysteresis in the M(H) loop becomes undetectably small. The decrease in pinning at $T_{irr}(H)$, results in a state with mobile vortices which are free to

dissipate. We have confirmed that $T_{fl}(H)$ coincides with $T_{irr}(H)$, by comparing dc magnetization with χ'' response measurements (cf. arrow marked as $T_{fl}= T_{irr}$ in Fig.8 for the 6.3 K curve). Thus $T_{fl}(H)$ coincides with $T_{irr}(H)$, which is also where the peak of the PE occurs, viz., the peak of PE at T_p occurs at the edge of irreversibility (cf. H-T phase diagram in Fig.9).

3.3 The H-T vortex phase diagram and pinning crossover region

Figure 9(a) shows the H - T, vortex matter phase diagram wherein we show the location of the $T_c(H)$ line which is determined by the onset of diamagnetism in $\chi'(T)$, the $T_p(B)$ line which denotes the location of the PE phenomenon, the $T_{cr}(H)$ line across which the $\chi''(T)$ response (shaded region 2 in Fig.5(c)) shows a substantial decrease in the dissipation and the T_{fl} line beyond which dissipation attempts to increase. The PE ceases to be a distinct noticeable feature beyond 750 G and the $T_p(H)$ line (identified with arrows in Fig. 5(a)) continues as the $T_{fl}(H)$ line. Note the $T_{fl}(H)$ line also coincides with $T_{irr}(H)$. For clarity we have indicated only the $T_{fl}(H)$ line in the phase diagram with open triangles in Fig.9(a).

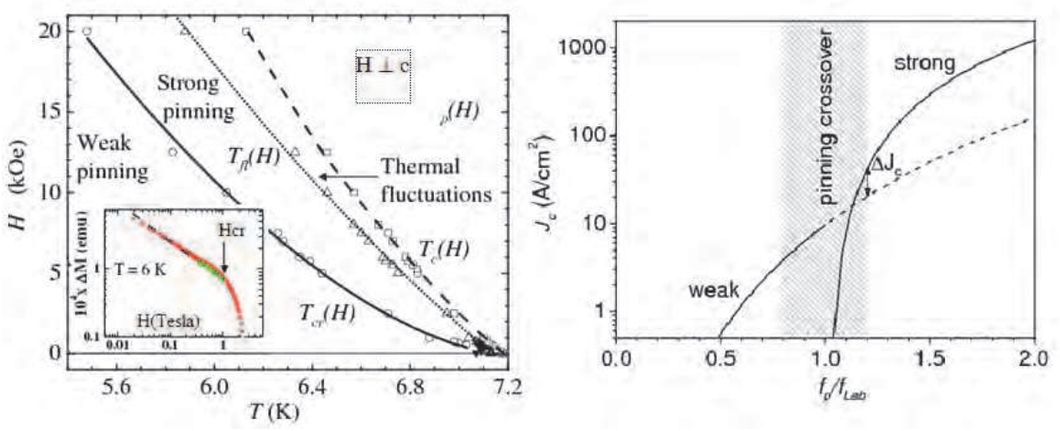

(a) (b)

Fig. 9. (a) The phase diagram showing the different regimes of the vortex matter. The inset is a log-log plot of the width of the hysteresis loop versus field at 6K. (b) An estimate of variation in J_c with f_p/f_{Lab} in different pinning regimes. [Mohan et al. 2007; Mohan 2009b].

We consider the $T_{cr}(H)$ line as a crossover in the pinning strength experienced by vortices, which occurs well prior to the PE. A criterion for weak to strong pinning crossover is when the pinning force far exceeds the change in the elastic energy of the vortex lattice, due to pinning induced distortions of the vortex line. This can be expressed as (Blatter et al, 2004), the pinning force (f_p) ~ Labusch force (f_{Lab}) = ($\varepsilon_0\xi/a_0$), where $\varepsilon_0 = (\phi_0/4\pi\lambda)^2$ is the energy scale for the vortex line tension, ξ is the coherence length, ϕ_0 flux quantum associated with a vortex, λ is the penetration depth and a_0 is the inter vortex spacing ($a_0 \propto H^{-0.5}$). A softening of the vortex lattice satisfies the criterion for the crossover in pinning. At the crossover in pinning, we have a relationship, $a_0 \approx \varepsilon_0\xi\ f_p^{-1}$. At $H_{cr}(T)$ and far away from T_c, if we use a monotonically decreasing temperature dependent function for $f_p \sim f_{p0}(1-t)^{\beta}$, where $t=T/T_c(0)$ and $\beta > 0$, then we obtain the relation $H_{cr}(T) \propto (1-t)^{2\beta}$. We have used the form derived for $H_{cr}(T)$ to obtain a good fit (solid line through the data Fig.9(a)) for $T_{cr}(B)$ data, giving $2\beta \sim 1.66 \pm 0.03$. Inset of Fig. 9(a) is a log-log plot of the width of the magnetization loop (ΔM)

versus H. The weak collective pinning regime is characterized by the region shown in the inset, where the measured ΔM(H) (red curve) values coincide with the black dashed line, viz., $\Delta M \propto J_c \propto 1/H^p$, with p as a positive integer (discussed earlier). Using expressions for $J_c(f_p/f_{Lab})$ (Blatter, 2004), $a_0 \sim \lambda$ and λ= 2300 A°, ξ= 23 A° for 2H-$NbSe_2$ (Higgins and Bhattacharya, 1996) and parameters like density of pins suitably chosen to reproduce J_c values comparable to those experimentally measured for 2H-$NbSe_2$, Fig.9(b) shows the enhancement in J_c expected at the weak to strong pinning regime, viz., around the shaded region in Fig.9(b) marked ΔJ_c, in the vicinity of $f_p/f_{Lab} \sim 1$. In Fig.9(a), the shaded region in the ΔM(H) ($\propto J_c(H)$, Bean, 1962; 1967) plot shows the excess pinning that develops due to the pinning crossover across $H_{cr}(T)$ ($\equiv T_{cr}(H)$). Comparing Figs.9(b) and 9(a) we find $\Delta Jc/J_{c,weak} \sim 1$ compares closely with the (change in ΔM in shaded region ~ 0.6 T in Fig.9(a) inset)/ ΔM (along extrapolated black line ~ 0.6 T) ~ 0.5. In the PE regime, usually $\Delta Jc/J_{c,weak} \geq 10$ (see for example in Fig.2). Note from the above analysis and the distinctness of the T_{cr} and T_p lines in Fig.9(a), shows that the excess pinning associated with the pinning crossover does not occur in the vicinity of the PE, rather it is a line which divides the elastically pinned regime prior to PE. Based on the above discussion we surmise that the $T_{cr}(H)$ line marks the onset of an instability in the static elastic vortex lattice due to which there is a crossover from weak (region 1 in Fig.5(c)) to a strong pinning regime (region 2 in Fig.5(c)). The crossover in pinning produces interesting history dependent response in the superconductor, as seen in the M_{rev} measurements of Fig. 8 and in the $\chi''(T)$ response for the ZFC and FC vortex states, in the main panel of Fig.7. In the inset (b) of Fig.8 we have schematically identified the pinning crossover (by the sketched dark curved arrows in Fig.8(b)) by distinguishing two different branches in the $M_{rev}(H)$ curve, which correspond to magnetization response of vortex states with high and low J_c. We reiterate that the onset of instability of the elastic vortex lattice sets in well prior to PE phenomenon without producing the anomalous PE.

As the strong pinning regime commences upon crossing H_{cr}, how then does pinning dramatically enhance across PE? The $T_{fl}(H)$ line in Fig.9 marks the end of the strong pinning regime of the vortex state. Above the $T_{fl}(H)$ line and close to $T_c(H)$, the tendency of the dissipation response to increase rapidly (Figs.1 and 2) especially at low H and high T, implies that thermal fluctuation effects dominate over pinning. We find that our values (H_{fl}, T_{fl}) in Fig.9(a), satisfies the equation governing the melting of the vortex state, viz., $B_{fl} = \beta_m \left(\frac{c_L^4}{G_i}\right) H_{c2}(0) \left(\frac{T_c}{T_{fl}}\right)^2 \left[1 - \frac{T_{fl}}{T_c} - \frac{B_{fl}}{H_{c2}(0)}\right]^2$, where, β_m = *5.6* (Blatter et al, 1994), Lindemann no. $c_L \sim 0.25$ (Troyanovski et al. 1999, 2002), $H_{c2}^{\perp c}(0)$ = 14.5 T, if a parameter, G_i is in the range of 1.5 x 10^{-3} to 10^{-4}. The Ginzburg number, G_i, in the above equation controls the size of the H - T region in which thermal fluctuations dominate. A value of $O(10^{-4})$ is expected for 2H-$NbSe_2$ (Higgins & Bhattacharya, 1996). The above discussion implies that thermal fluctuations dominate beyond $T_{fl}(H)$. By noting that $T_p(H)$ appears very close to $T_{fl}(H)$, it seems that PE appears on the boundary separating strong pinning and thermal fluctuation dominated regimes.

The above observations (Mohan et al, 2007) imply that instabilities developing within the vortex lattice lead to the crossover in pinning which occurs well before the PE. Infact, PE

seems to sit on a boundary which separates a strong pinning dominated regime from a thermal fluctuation dominated regime. These assertions could have significant ramifications pertaining to the origin of PE which was originally attributed to a softening of the elastic modulii of the vortex lattice. Even though thermal fluctuations try to reduce pinning, we believe newer results show that at PE, the pinning and thermal fluctuations effects combine in a non trivial way to dramatically enhance pinning, much beyond what is expected from pinning crossovers. The change in the pinning response deep in the elastic vortex state is expected to lead to nonlinear response under the influence of a drive. It is interesting to ask if these crossovers and transformation in the static vortex state evolve and leave their imprint in the driven vortex state.

4 Nonlinear response of the moving vortex state

4.1 I-V characteristics and the various phases of the driven vortex matter

In the presence of an external transport current (I) the vortex lattice gets set into motion. A Lorentz force, $\mathbf{f_L=J \times \phi_0/c}$, acting on each vortex due to a net current density J (due to current (I) sent through the superconductor and the currents from neighbouring vortices) sets the vortices in motion. As the Lorentz force exceeds the pinning force, i.e $f_L>f_p$, the vortices begin to move with a force-dependent velocity, v. The motion of the flux lines induces an electric field $\mathbf{E = B \times v}$, in the direction of the applied current causing the appearance of a longitudinal voltage (V) across the voltage contacts (Blatter et al, 1994). Hence, the measured voltage, V in a transport experiment can be related to the velocity (v) of the moving vortices via V=Bvd, where d is the distance between the voltage contacts. Measurements of the V (equivalent to vortex velocity v) as a function of I, H, T or time (t) are expected to reveal various phases and their associated characteristics an nonlinear behavior of the driven vortex state.

When vortices are driven over random pinning centers, broadly, four different flow regimes have been established theoretically and through significantly large number of experiments (Shi & Berlinski 1991; Giammarchi & Le Doussal, 1996; Le Doussal & Giammarchi, 1998; Giammarchi & Bhattacharya, 2002). These are: (a) depinning, (b) elastic flow, (c) plastic flow, and (e) the free-flow regime. At low drives, the depinning regime is first encountered, when the driving force just exceeds the pinning force and the vortices begin moving. As the vortex state is set in motion near the depinning regime, the moving vortex state is proliferated with topological defects, like, dislocations (Falesky et al, 1996). As the drive is increased by increasing the current through the sample, the dislocations are found to heal out from the moving system and the moving vortex state enters an ordered flow regime (Giammarchi & Le Doussal, 1996; Yaron et al., 1994; Duarte, 1996). The depinning regime is thus followed by an elastically flowing phase at moderately higher drives, when all the vortices are moving almost uniformly and maintain their spatial correlations. The nature and characteristics of this phase was theoretically described as the moving Bragg glass phase (Giammarchi & Le Doussal, 1996; Le Doussal & Giammarchi, 1998). In the PE regime of the H- T phase diagram, it is found that as the vortices are driven, the moving vortex state is proliferated with topological defects and dislocations, thereby leading to loss of correlation amongst the moving vortices (Falesky et al, 1996; Giammarchi & Le Doussal, 1996; Le Doussal & Giammarchi, 1998; Giammarchi & Bhattacharya 2002). This is the regime of plastic flow. In the plastic flow regime, chunks of vortices remain pinned forming islands of localized vortices, while there are channels of moving vortices flowing around these pinned islands, viz., different parts of the system flow with different velocities

(Bhattacharya & Higgins, 1993, Higgins & Bhattacharya 1996; Nori, 1996; Tryoanovski et al, 1999). The effect of the pins on the moving vortex phase driven over random pinning centers is considered to be equivalent to the effect of an effective temperature acting on the driven vortex state. This effective temperature has been theoretically considered to lead to a driven vortex liquid regime at large drives (Koshelev & Vinokur, 1994). At larger drives, the vortex matter is driven into a freely flowing regime. Thus, with increasing drive, interplay between interaction and disordering effects, causes the flowing vortex matter to evolve between the various regimes.

The plastic flow regime has been an area of intense study. The current (I) - voltage (V) characteristics in the plastic flow regime across the PE regime are highly nonlinear (Higgins & Bhattacharya, 1996), where a small change in I is found to produce large changes in V. Investigations into the power spectrum of V fluctuations revealed significant increase in the noise power on entering the plastic flow regime (Marley, 1995; Paltiel et al., 2000, 2002). The peak in the noise power spectrum in the plastic flow regime was reported to be of few Hertz (Paltiel et al., 2002). The glassy dynamics of the vortex state in the plastic flow regime is characterized by metastability and memory effects (Li et al, 2005, 2006; Xiao et al, 1999). An edge contamination model pertaining to injection of defects from the nonuniform sample edges into the moving vortex state can rationalise variety of observations associated with the plastic flow regime (Paltiel et al., 2000; 2002). In recent times experiments (Li et al, 2006) have established a connection between the time required for a static vortex state to reach steady state flow with the amount of topological disorder present in the static vortex state. By choosing the H-T regime carefully, one finds that while the discussed times scales are relatively short for a well ordered static vortex state, the times scales become significantly large for a disordered vortex state set into flow, especially in the PE regime. The discovery of pinning transformations deep in the elastic vortex state (Mohan et al, 2007), motivated a search for nonlinear response deep in the elastic regime as well as to investigate the time series response in the different regimes of vortex flow (Mohan et al, 2009).

4.2 Identification of driven states of vortex matter in transport measurements

The single crystal of 2H-$NbSe_2$ used in our transport measurements (Mohan et al, 2009) had pinning strength in between samples of A and B variety (see section 2.1.1). The dc magnetic field (H) applied parallel to the c-axis of the single crystal and the dc current (I_{dc}) applied along its 'ab' plane (Mohan et al, 2009). The voltage contacts had spacing of d ~ 1 mm apart. Figure 10(a) shows the plots of resistance ($R=V/I_{dc}$) versus H at 2.5 K, 4 K, 4.5 K, 5 K, 5.8 K and 6 K measured with I_{dc}=30 mA. With increasing H, all the R-H curves exhibit common features viz., nearly zero R values at lowest H, increasing R after depinning at larger H, an anomalous drop in R associated with onset of plastic flow regime and finally, a transition to the normal state at high values of H. To illustrate in detail these main features, and to identify different regime of driven vortex state, we draw attention only to the 5 K data in Figure 10(b).

At 5 K, for H < 1.2 kOe, R < 0.1 mΩ, which implies an immobile, pinned vortex state. Beyond 1.2 kOe (position marked as H_{dp} in Fig.10(b)), the FLL gets depinned and R increases to mΩ range. From this we estimate the critical current I_c to be 30 mA (at 5 K, 1.2 kOe). The enhanced pinning associated with the anomalous PE phenomenon leads to a drop in R starting at around 6 kOe (onset location marked as H_{pl}) and continuing up to around 8 kOe (location marked as H_p). The PE (≡ plastic flow) region is shaded in Fig.10(b). As

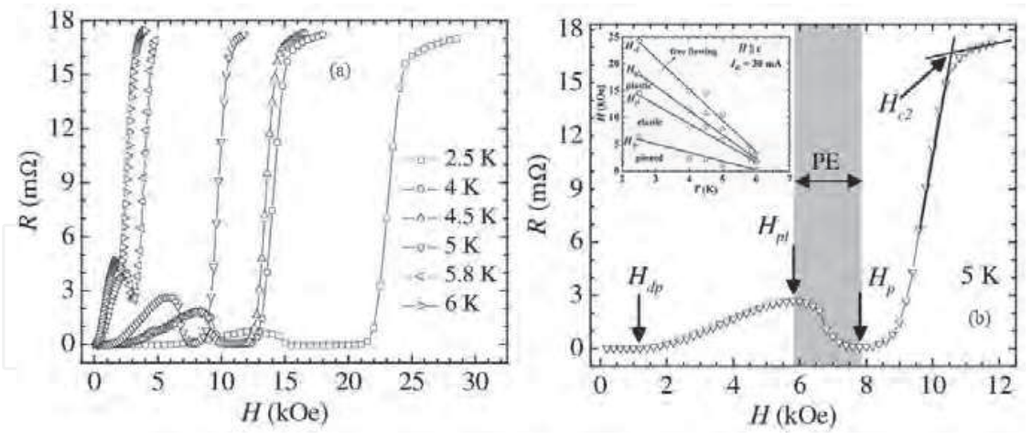

Fig. 10. (a) R versus H (H \\ c) of the vortex state, measured at different T with I_{dc}=30 mA. (b) R-H at 5 K only, with the different driven vortex state regimes marked with arrows. The arrows marks the locations of, depinning (H_{dp}), onset of plastic deformations (H_p), peak location of PE (H_p) and upper critical field (H_{c2}) at 5 K, respectively. The inset location of above fields (Fig.10(b)) on the H-T diagram. [Mohan et al. 2009a; Mohan 2009b].

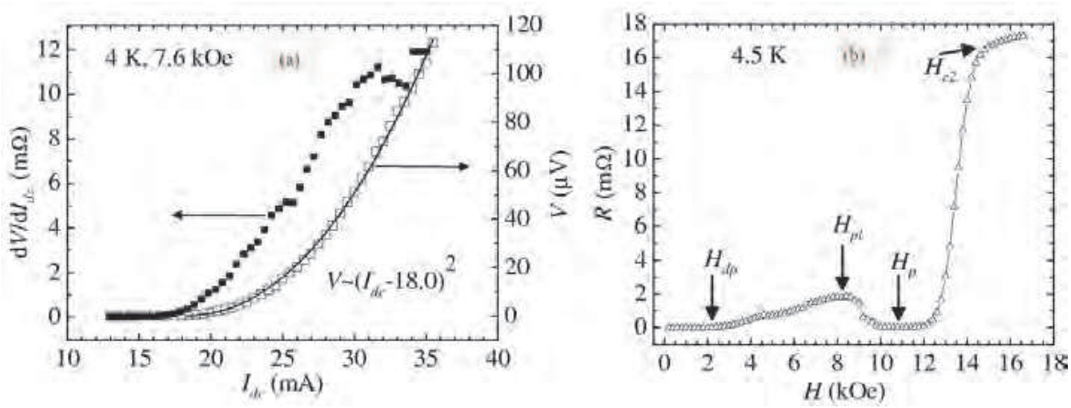

Fig. 11. (a) The V-I_{dc} characteristics and dV/dI_{dc} vs I_{dc} in the elastic phase at 4 K and 7.6 kOe. The solid line is a fit to the V-I_{dc} data, (cf. text for details). (b) R-H curve at 4.5 K and I_{dc}= 30 mA. [Mohan et al. 2009a; Mohan 2009b]

discussed earlier (Fig.9), beyond H_p, thermal fluctuations dominate causing large increase in R associated with pinning free mobile vortices until the upper critical field H_{c2} is reached. We determine $H_{c2}(T)$ as the intersection point of the extrapolated behaviour of the R-H curve in the normal and superconducting states, as shown in Fig.10(b). By identifying these features from the other R-H curves (Fig.10(a)), an inset in Fig.10(b) shows the H-T vortex phase diagram for the vortex matter driven with I_{dc} = 30 mA.

Figure 11 shows the V-I_{dc} characteristics at 4 K and 7.6 kOe; this field value lies between $H_{dp}(T)$ and $H_{pl}(T)$ (see inset, Fig.10(b)), i.e. in the elastic flow regime. It is seen that the data fits (see solid line in Fig.11(a)) to $V\sim(I_{dc} - I_c)^{\beta}$, where $\beta \sim 2$ and I_c = 18 mA ($I = I_c$, when $V \geq 5$ μV, as V develops only after the vortex state is depinned), which inturn indicates the onset of an elastically flow. Experiments indicate the concave curvature in I-V coincides with ordered elastic vortex flow (Duarte et al, 1996; Yaron et al.,1994; Higgins and Bhattacharya 1996). Unlike the elastic flow regime, the plastic flow regime is characterized by a convex

curvature in the V-I_{dc} curve alongwith a conspicuous peak in the differential resistance (Higgins and Bhattacharya, 1996), which is absent in Fig.11 (see dV/dI_{dc} vs I_{dc} in Fig.11(a)). All the above indicate ordered elastic vortex flow regime at 4 K, 7.6 kOe and I = 30 mA. The dV/dI_{dc} curve also indicates a nonlinear V-I_{dc} response deep in the elastic flow regime.

4.3 Time series measurements of voltage fluctuations and its evolution across different driven phases of the vortex matter

Figure 11(b), shows the R-H curve for 4.5 K. Like Fig.10(b), in Fig. 11 (b), the H_{dp}, H_{pl}, H_p and H_{c2} locations are identified by arrows, which also identify the field values, at which time series measurements were performed. The protocol for the time series measurements was as follows: At a fixed T, H and I_{dc}, the dc voltage V_0 across the electrical contacts of the sample was measured by averaging over a large number of measurements ~ 100. The V_0 measurement prior to every time series measurement run, ensures that we are in the desired location on R-H curve, viz., the V_0/I value measured before each time series run should be almost identical to the value on the R(H) curve at the given H,T, like the one shown in Figs.10(b) or 11(b). After ensuring the vortex state has acquired a steady flowing state, viz., by ensuring the mean V,i.e., <V> ~ V_0, the time series of the voltage response (V(t)) is measured in bins of 35 ms for a net time period of a minute, at different H, T.

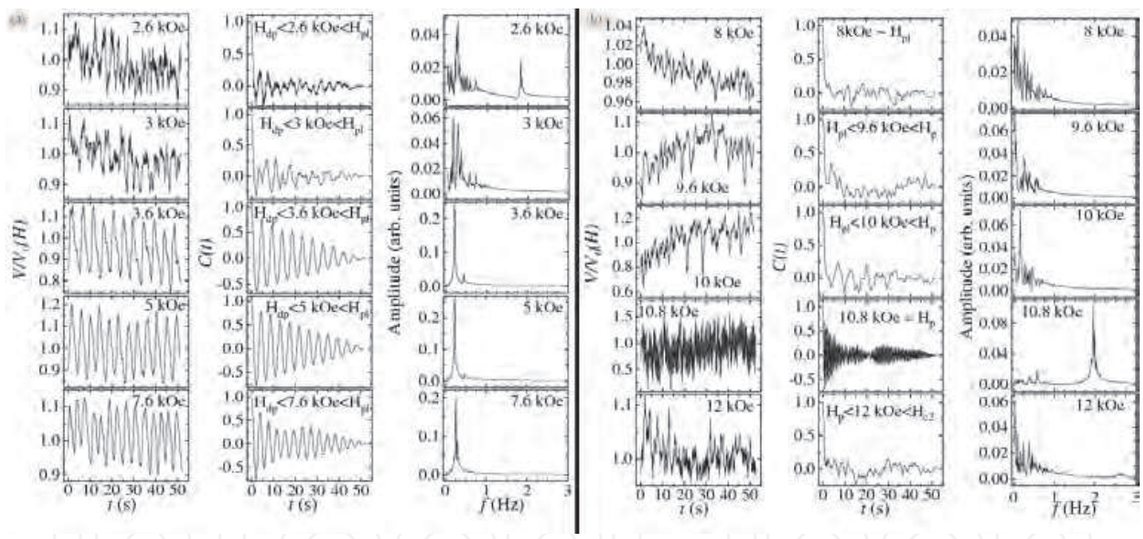

Fig. 12. (a) The left most vertical column of panels represent the fluctuations in voltage $V(t)/V_0$ measured at different fields at 4.5 K with I_{dc} of 30 mA. Note: V_0(2.6 kOe) = 1.4 μV, V_0(3 kOe) = 3.7 μV, V_0(3.6 kOe) = 9.5 μV, V_0(5 kOe) = 21.1 μV, V_0(7.6 kOe) = 50.7 μV. The middle set of panels are the C(t) calculated from the corresponding $V(t)/V_0$ panels on the left. The right hand set of panels show the amplitude of the FFT spectrum calculated from the corresponding C(t) panels. In Fig.12 (b), the organization of panels is identical to that in Fig.12 (a) with, V_0(8 kOe) = 54.5 μV, V_0(9.6 kOe) = 9.8 μV, V_0(10 kOe) = 1.0 μV, V_0(10.8 kOe) = 0.2 μV, V_0(12 kOe) = 3.2 μV. [Mohan et al. 2009a; Mohan 2009b]

The time series V(t) measurements at T=4.5 K are summarised in Figs.12 (a), Fig.12 (b), Fig. 13 (a) and Fig.13 (b). The stack of left hand panels in Figs. 12(a), 12(b), 13(a) and 13(b) show the normalized $V(t)/V_0$ versus time (t) for different driven regimes, viz., the just depinned state (H ~ H_{dp}), the freely flowing elastic regime (H_{dp} <H < H_{pl}), above the onset of the

plastic regime ($H > H_{pl}$), deep inside the plastic regime ($H \sim H_p$) and above PE regime ($H > H_p$) (cf. Fig.11(b)). A striking feature in these panels is the amplitude of fluctuations in V(t) about the V_0 value are significantly large, varying between 10-50% of V_0, depending on the vortex flow regime. As one approaches very near to the normal regime, the fluctuations in V(t) are about 1% of V_0 (see bottom most plot at 16 kOe the left stack of panels in Fig.13(a)) and is about 0.02% deep inside the normal state (see Fig. 13(b), left panel). Near H_{dp} (2.6 kOe and 3 kOe, Fig.12(a)) the fluctuations are not smooth, but on entering the elastic flow regime, one can observe spectacular nearly-periodic oscillations of V(t) (see at 3.6 kOe, 5 kOe and 7.6 kOe in panels of Fig.12(a)). Such conspicuously large amplitude, slow time period fluctuations of the voltage V(t), which are sustained within the elastically driven state of the vortex matter (up to 7.6 kOe), begin to degrade on entering the plastic regime (above 8 kOe, see Fig.12(b)).

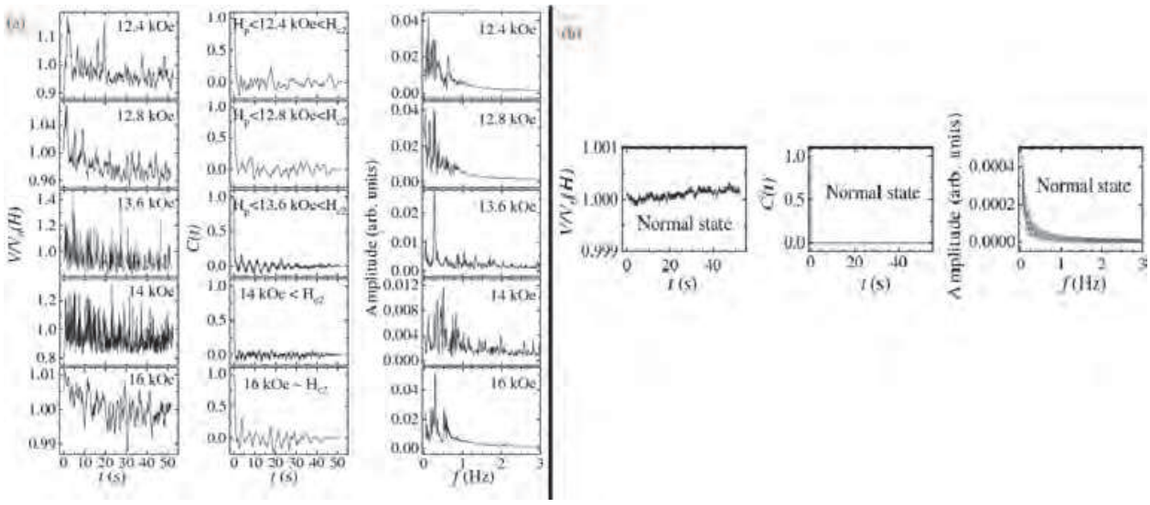

Fig. 13. (a) consists of three columns representing $V(t)/V_0$, C(t) and power spectrum of fluctuations (see text for details) measured with I_{dc} of 30 mA. Note: V_0(12.4 kOe) = 13.6 μV, V_0(12.8 kOe) = 49.6 μV, V_0(13.6 kOe) = 284.9 μV, V_0(14 kOe) = 404.5 μV, V_0(16 kOe) = 513.7 μV. (b)Panels show similar set of panels as (a) in the normal state at T = 10 K and H = 10 kOe with I_{dc} of 30 mA (V_0 = 539. 6 μV). [Mohan et al. 2009a; Mohan 2009b]

Considering that the voltage (V) developed between the contacts on the sample is proportional to the velocity (v) of the vortices (see section 4.1, V=Bvd), therefore to investigate the velocity – velocity correlations in the moving vortex state, the voltage-voltage (≡ velocity – velocity) correlation function: $C(t) = \frac{1}{V_0^2}\langle V(t'+t)V(t)\rangle$, was determined from the $V(t)/V_0$ signals (see the middle sets of panels in Figs.12 (a) and 12 (b) and Fig. 13 for the C(t) plots). In the steady flowing state, if all the vortices were to be moving uniformly, then the velocity – velocity correlation (C(t)) will be featureless and flat. While if the vortex motion was uncorrelated then they would lose velocity correlation within a short interval of time after onset of motion, then the C(t) would be found to quickly decay. Note an interesting evolution in C(t) with the underlying different phases of the vortex matter. While there are almost periodic fluctuations in C(t) at 3.6 kOe, 5 kOe and 7.6 kOe (at $H < H_{pl}$) sustained over long time intervals, there are also intermittent quasi-periodic

fluctuations sustained for a relatively short intervals even at H > H_{pl}, viz., at 10.8 kOe and 13.6 kOe (see Fig.12 and Fig.13). The periodic nature of C(t) indicates that in certain regimes of vortex flow, viz., even deep in the driven elastic regime (viz., 3.6 kOe, 5 kOe and 7.6 kOe in Fig.12(a) panels) the moving steady state of the vortex flow, the vortices are not always perfectly correlated. Instead their velocity appears to get periodically correlated and then again drops out of correlation.

Once can deduce the power spectrum of the fluctuations by numerically determining the fast Fourier transform (FFT) of C(t). The FFT results are presented in the right hand set of panels in Figures 12(a), 12(b), 13(a) and 13(b). A summary of the essential features of the power spectrum are as follows. At 2.6 kOe where the vortex array is just above the depinning limit for I_{dc} = 30 mA, one finds two peak-like features in the power spectrum centered around 0.25 Hz and 2 Hz (Fig.12(a)). With increasing field, the peak feature at 2 Hz vanishes, and with the onset of freely flowing elastic regime (>3 kOe), a distinct sharp peak located close to 0.25 Hz survives. This low-frequency peak, which exists up to H = 7.6 kOe, has an amplitude nearly five times that at 0.25 Hz for 2.6 kOe. In the plastic flow regime, viz., H > H_{pl} ~ 8 kOe, the amplitude of the 0.25 Hz frequency starts diminishing (Figs.12(b), the right most panel). At the peak location of the PE (H_p=10.8 kOe), the 0.25 Hz frequency is absent but there is now a well defined peak in the power spectrum close to 2 Hz (see Fig.12(b)). Close to the vortex state depinning out of the plastic regime (i.e., close to the termination of PE (e.g., at 12.4 kOe and beyond, in Fig.13(b)), the 2 Hz peak dissappears and a broad noisy feature, which seems to be peaked, close to mean value ~ 0.25 Hz makes a reappearance (cf. right hand panels set in Fig.13(a)).

Close to 13.6 kOe and 14 kOe, one finds that the fluctuations begin to appear at multiple frequencies, indicating a regime of almost random and chaotic regime of response. Features related to a chaotic regime of fluctuations are being described later in section 4.6. As one begins to approach close to H_{c2}, i.e., at 16 kOe, one observes a broad spread out spectrum with weak amplitude. For the sake of comparison, in the panels in Fig.13(b), the measured and analyzed $V(t)/V_0$, C(t) and the power spectrum of voltage fluctuations in the normal state of the superconductor at 10 K and 10 kOe stand depicted. Note that the V(t) is just abut 0.02% of V_0, which is far lower than that present in the superconducting state. The C(t) is featureless and the power spectrum of the fluctuations in the normal state also does not show any characteristics peak in the vicinity of 0.25 Hz or 2 Hz.

The evolution in the fluctuations described above at T=4.5 K is also found at other temperatures. Similar to 4.5 K measurements of the voltage – time series were done at 2.5 K, 5 K, 5.8 K, 6 K (Mohan, 2009b). Figure 14 shows the power spectrum of the fluctuations in V recorded at 2.5 K in different field regimes (Mohan, 2009a). Panel (a) of Fig.14 shows the R-H behavior plot for T=2.5 K, where the field locations of H_{dp}, H_{pl}, H_p and H_{c2} have been marked with arrows. By comparing the power spectrum of fluctuations at 2.5 K (Figs.14 (a) and 14(b)) with those at 4.5 K (the left most set of panels in Figs.12(a), 12(b) and 13(a)), one can find similarity in overall features, along with some variations as well. For example, note that like at 4.5 K, in 2.5 K also, just after depinning, the vortex state viz., at 6. 5 kOe at 2.5 K (Fig.14) and 2.6 kOe at 4.5 K (Fig.12(a)), one can observe the presence of two discernable features in the power spectrum located in the vicinity of the 0.2 Hz and 2.25 Hz. However, unlike at 4.5 K where the peak at 2 Hz quickly disappeared by 3 kOe (Fig.12(a)) at 2.5 K on moving to fields away from the H_{dp}, the two peak structure (one close to 0.2 Hz and another close to 2.25 Hz) in the power spectrum persists upto field of 12. 5 kOe (see Fig.14(b)). At 2.5 K the peak located near 2.25 Hz in the power spectrum progressively decreases with increasing H until it

dissapears at 13.5 kOe and only a broad feature with peaks in the sub- Hertz regime remains (see, 13.5 kOe and 14.5 kOe data in the panels of Fig.14(c)). Unlike at 4.5 K, where the periodic nature of the fluctuations in the ordered elastic flow regime was clearly discernable, at 2.5 K the fluctuations in V(t) are not as periodic (perhaps due to the admixture of the two characteristic frequencies). Here one can argue that both drive and thermal fluctuation effects play a significant role in generating the characteristic fluctuations. At 2.5 K, on entering the PE regime, similar to 4.5 K data, one finds only find a lone peak surviving near 2 Hz in the power spectrum of fluctuations (compare 18 kOe data at 2.5 K in Fig.14(c) panel with the 10.8 kOe data in Fig.12(b)). Beyond the PE regime at 22 kOe at 2.5 K only the broad feature in the sub-Hertz regime survives. At other higher T (> 4.5 K and close to $T_c(H)$) the features in the power spectrum are almost identical to those seen for 4.5 K with the difference being that features in the sub-Hertz regime become dominant compared to the Hertz regime (Mohan, 2009).

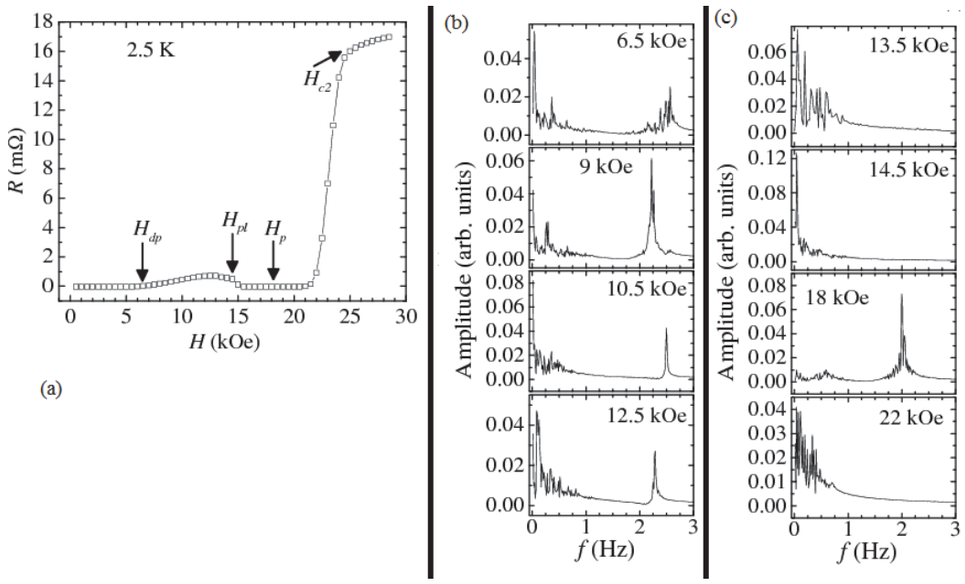

Fig. 14. (a) R–H behavior at 2.5 kOe measured with I_{dc} = 30 mA. Panels (b) and (c) represent the power spectrum of fluctuations at 2.5 K at different H. [Mohan 2009b]

4.4 Excitation of resonant like modes of fluctuations in the driven vortex phase

The above measurements have revealed that a dc drive (with I_{dc}) excites large fluctuations in voltage (equivalent to velocity) in the range of 10 – 40% of the mean voltage level (V_0) at characteristic frequencies (f_0 and f'_0) located in the range of 0.2 Hz and 2 Hz, respectively. The observation that low-frequency modes can get excited in the driven (by I_{dc}) vortex lattice had led Mohan et al, (2009) to explore the effect of a small ac current (I_{ac}) superimposed on I_{dc}, where the external periodic drive with frequencies (f) close to f_0 and f'_0 may result in a resonant like response of the driven vortex medium. The vortex lattice was driven with a current, $I = I_{dc} + I_{ac}$, where $I_{ac} = I_0 Cos(2\pi ft)$ is the superposed ac current on I_{dc}. At 4 K at different H, the vortex state is driven with I(f), and the dc voltage V of the sample was measured while varying the f of $I_{ac}(f)$. Figure 15 shows the measured V against f at different values of H, where I_{dc} = 22 mA and I_0 = 2.5 mA ($I_{ac} = I_0 Cos(2\pi ft)$), where the I_0 is chosen to ensure that $I_{dc}+I_0$ gives the same V as with only I_{dc} = 30 mA, at the given H,T.

In the elastic regime (7.6 kOe, cf. Fig. 15(a)) one observes spectacular oscillations in V(f). Significantly large oscillations are observed in V at low f , viz., f < 3 Hz, where the oscillations can exceed (by nearly 100%) of the mean V level determined by the I_{dc}. Shown in Fig.15(b) is an enlarged view of the low-f region of the V(f) data at 7.6 kOe presented in Fig.15(a). An important feature to note in Fig. 15(b) is the enhanced regimes of fluctuations in V(f) occurring at the harmonics of 0.25 Hz (see arrows in bold in Fig.15(b)).

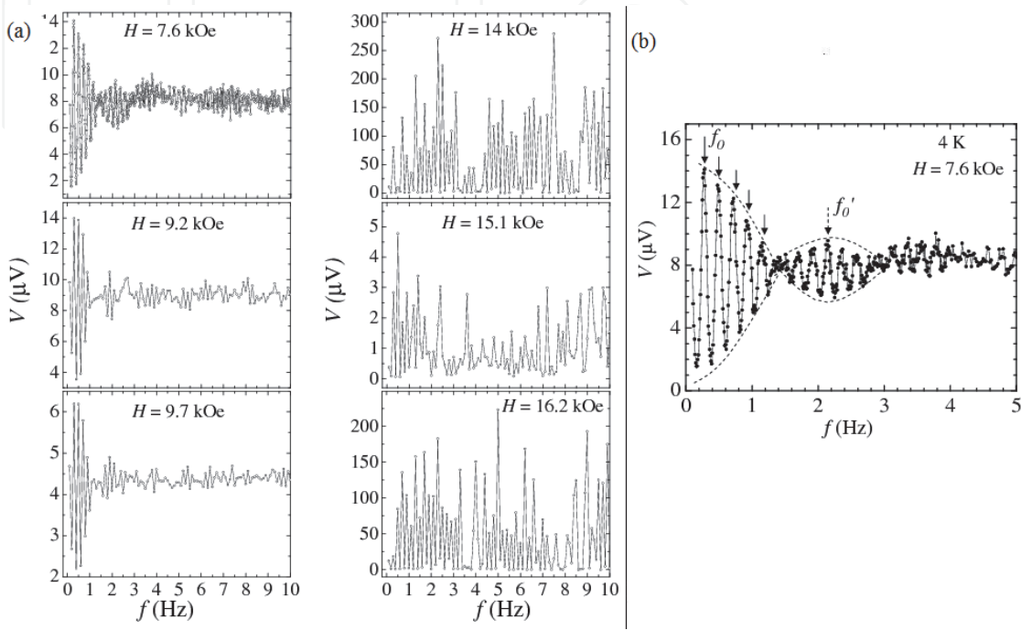

Fig. 15. (a) The measured dc voltage V against frequency f of I_{ac} at different values of H at 4 K and with a current $I = I_{dc} + I_{ac}$, where I_{dc} = 22 mA and I_0 = 2.5 mA. (b) An enlarged view of V(f) at 4 K and 7.6 kOe (panel (a)). The arrows in 'bold' mark the location of the resonant peaks in V(f). [Mohan et al. 2009a; Mohan 2009b]

Note that the peak of the fluctuations in V(f) at the harmonics of 0.25 Hz appears to follow an envelope curve, which has a frequency of 2 Hz (see envelope curve in Fig.15(b)), though the envelope of fluctuation at f_0' ~ 2 Hz damps out faster than that at f_0~ 0.25 Hz. However, one can see that f of I_{ac} matches with the characteristic frequencies f_0 and f'_0 (cf Figs. 12 and 13), which are excited with I_{dc}, viz., ~ 0.25 Hz and ~ 2 Hz, where one observes resonant oscillations in the V. Note that by increasing H as one enters the plastic regime, for example at 9.2 kOe (Fig.15(a)), the enhanced resonant like fluctuations in V(f) at the harmonics of 0.25 Hz seem to rapidly diminish. At 7.6 kOe, while one observes resonant like fluctuations in V(f) upto $6f_0$, f_0 = 0.25 Hz, at 9.2 kOe, one observes the same till only about $4f_0$. Notice that above the peak of the PE, viz., at 14 kOe and beyond, one observes no resonant like behavior in V(f), instead the system seems to exited at all frequencies, which is indicative of a chaotic regime of fluctuations. It is interesting to note similar behavior was also observed in the power spectrum of fluctuations in the vortex velocity excited at 14 kOe in Fig.13(a). Thus, the observation of large (~100%) excursions in the measured V_{dc} signal at harmonics of 0.25 Hz indicates a significantly large *nonlinear* response in the traditionally assumed *linear*, weakly disordered - driven vortex solid prior to the PE. The above chaotic behavior continues well above the onset of the PE regime. Though from the earlier discussion of Figs.

12 and 13, it may have appeared that f_0 ~ 0.2 – 0.25 Hz makes a comeback above the PE, leading one to propose a similarity of driven phases before and above the PE, yet the present measurements indicate that above PE, the f_0 does not excite the resonant like feature which are characteristic of f_0 deep in the elastic regime (viz., see Fig.15).

It has been proposed (Mohan et al, 2009a) that the resistance of the sample varies as, $R = R_0 \pm \sum_{n=1}^{m} [R_n Cos(n2\pi f_0 t) + R_n^{/} Sin(n2\pi f_0 t)]$,under the influence of current, $I = I_{dc} + I_{ac.}$ Here, R_0 is the resistance of the sample in response to the I_{dc} alone, R_n and $R_n/$ are the f dependent coefficients of the in-phase and out-of-phase responses, and f_0 is the characteristic frequency of fluctuations. The f_0 (= 0.25 *Hz*) corresponds to the peak value in the power spectrum for H = 7.6 kOe and T = 4.5 K in Fig.15(b). Taking the time average of the expression, $V = IR$, yields, $V_{dc} = I_{dc}R_0 \pm (I_0R_n)/2$, at $f = nf_0$. From the very large fluctuations (~100%) seen in Fig.15, it is clear that $(I_0R_1)/2 \approx I_{dc}R_0$ or $R_1 \sim 20\ R_0$, is a substantially large component excited at f = f_0. Similarly, at f = 2 f_0, $R_2 \sim 15\ R_0$. Notice from Fig.15, that the nonlinear response can be easily seen upto f = 5 to $6f_0$ (see the positions of solid arrows in Fig.15(b)). The envelope of the amplitude of fluctuations in Fig.15(b) appears to decrease upto 5 f_0; thereafter, the envelope regenerates itself into second and third cycles of oscillations, but, with progressively, reduced intensities. Thus, a small perturbation with $I_{ac} \sim 0.1\ I_{dc}$ triggers large fluctuations along with a higher-harmonic generation indicating a highly nonlinear nature of the dynamics. It is noteworthy that the envelope of the resonant oscillations at nf_0 seen at 7.6 kOe with a frequency of 2 Hz (= f'_0) is damped out in the plastic regime. Thus, the peak in the vicinity of f_0'=2 Hz as seen in Figs.12, 13 and 14, have properties different from f_0 ~ 0.2 – 0.25 Hz. Unlike f_0, the $I_{ac}(f_0')$ does not excite resonant like modes of fluctuations especially in the plastic regime, and even in the elastic regime as noted earlier the envelope (dotted curve in Fig.15(b)) with frequency f_0' = 2 Hz damps out very quickly. Thus f_0 and f_0' are associated with distinct behavior of different states of the driven vortex matter.

4.5 Evolution in the characteristic frequencies observed in the power spectrum with vortex velocity

It is known that the periodically spaced vortices when driven over pins, lead to a specific variety of vortex-velocity fluctuations, called the washboard frequency (Fiory 1971; Felming & Grimes 1979; Harris et al., 1995; Kokubo et al, 2005), which are in the range of 0.1-1 MHz. The wash board frequency is far larger than the frequencies, elucidated above. It has also been reported that the nonlinear *I-V* characteristics in the PE regime is accompanied with low frequency noise (<< washboard frequency) in the range of few Hz (Higgins and Bhattacharya 1996; Paltiel et al, 2000; 2002; Gordeev et al 1997; Marley et al 1995; Merithew et al. 1996). The peak in the noise power density in the vicinty of 3 Hz in the PE regime in 2H-$NbSe_2$ was rationalized within the edge contamination framework (Paltiel et al., 2000;2002). Qualitatively, as per the edge contamination model (Paltiel et al, 2000; 2002), the disordered vortices injected from irregularities on the sample boundaries lead to a slow down of the ordered vortices driven inside the sample. This causes a reduction in the injection rate of the disordered vortices. As the fraction of the injected disordered vortices decreases, the velocity of the driven state inturn increases and the entire process repeats. This is the source of velocity fluctuations via the edge contamination picture. It has been argued that edge contamination should result in velocity fluctuations, which are proportional to the rate of injection of vortices which typically are in the range few Hz. In our case, vortices need about 0.1 s to traverse the typical

width of our sample of ~ 0.1 cm, with a vortex velocity , v = <V(t)>/(d.B) ~ 10^{-2} m/s(= 1 cm/s), where V ~ 10 μV observed at 30 mA, B =μ_0H = 1 Tesla, and d is the distance between the electrical contacts = 10^{-3} m. Therefore, the injection rate of disordered vortices into the moving vortex medium from irregularities at the sample edges is at the rate of ~ 10 Hz. The observation of a peak in the velocity fluctuation spectrum centered around 2 Hz (cf. Figs. 12, 13 and 14) in the PE region could be termed as consistent with earlier reported observations of peak in noise power in similar frequency range in the PE regime of $NbSe_2$ (Paltiel et al., 2002; Merithew et al., 1996) and $YBa_2CuO_{7-\delta}$ (Gordeev et al., 1997). However, in the ordered elastic driven vortex state prior to PE, one also notes a much lower frequency of 0.25 Hz (cf. Figs.12, 13 and 14), which as per the edge contamination model would imply an effective sample width of 4 cm (with u = 1 cm/s), which would be >> actual sample width (~ 0.1 cm). This implies a deviation from the edge contamination picture.

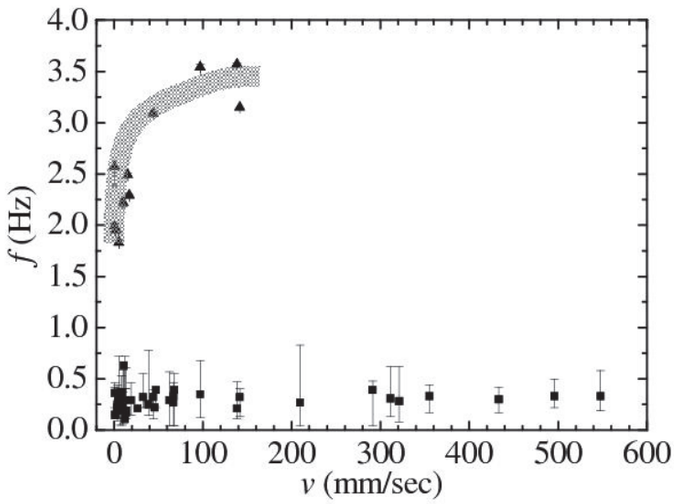

Fig. 16. The evolution of the characteristic frequencies associated with fluctuations in vortex motion as a function of velocity of vortices. The shaded band represents the behaviour of the higher characteristic frequency. [Mohan et al. 2009a; Mohan 2009b]

Figure16 shows an evolution in f_0 (~ 0.05 H_z, solid squares) and f'_0 (~ 2 Hz, solid triangles) with velocity (v) of the vortices (Mohan et al, 2009). This compilation is based on measurements at different H, T, and I_{dc}. One can see that the higher characteristic frequency f_0' increases with v, varying from around 1.75 Hz to 3.5 Hz, while the lower f_0 is v independent. This is consistent with the impression from the I_{dc}+I_{ac} experiments that f_0 and f_0' have distinct behavior and do not correspond to part of the same behavior repeating at different frequencies. From the conventional noise mechanism, based on edge contamination model, one would expect the frequency of v fluctuations (equivalent to the disorder injection rate) to increase with v without showing any tendency to saturate with v. However, this is not the case as seen in Fig.16. While the higher frequency f_0'does seem to increase with v at lower values (see shaded region in Fig.16), it shows a much more slower change with v at higher values, with a tendency to saturate. The lower frequency appears to be nominally v independent, which is unexpected within edge contamination model. One may clarify that in certain v regimes only one of the two frequencies survives. It can be stated that the detailed richness of

the fluctuations in the descriptions presented here do not find a rationalization within the present models relating to noise in the driven vortex state.

The current understanding of the nature of the flowing vortex state and transitions within it are inadequate. This is best illustrated by the nonlinear nature of the response within the steady state of driven elastic vortex medium (cf. discussion pertaining to Figs.12 – 16 above), which is far from the conventional notion that the elastic medium is almost a benign medium, which responds almost linearly to drive. Infact though a lot has been understood regarding the plastic flow regime (see discussion relating to the plastic flow regime in section 4.1), newer works (Olive & Soret, 2006; 2008) have indicated that the vortices in this regime exhibit chaotic regimes of flow, where the velocity fluctuations of the vortices may show intermittent velocity bursts which can be a route for the emergence of chaos in the vortex state.

4.6 Intermittent voltage bursts in driven vortex state

The nature of voltage fluctuations and the associated power spectrum of fluctuations at 4.5 K (cf. Fig.13(a), 14 kOe data) reveal that in the regime just after PE the vortices driven by a dc drive (I_{dc}) begin to exhibit v fluctuations at all possible frequencies. This behavior is further corroborated by the V(f) data in Fig.15, which shows that the vortex state at 14 kOe (just above the PE regime) when driven with I_{dc} and perturbed with $I_{ac.}$ The driven vortex state at 14 kOe begins to show large nonlinear excursion in v (equivalent to V) at all f in the range over which f is varied. Such a behavior, where the nonlinear fluctuations in v exists uniformly over a large frequency interval is indicative of the onset of a chaotic regime of flow in the vortex state.

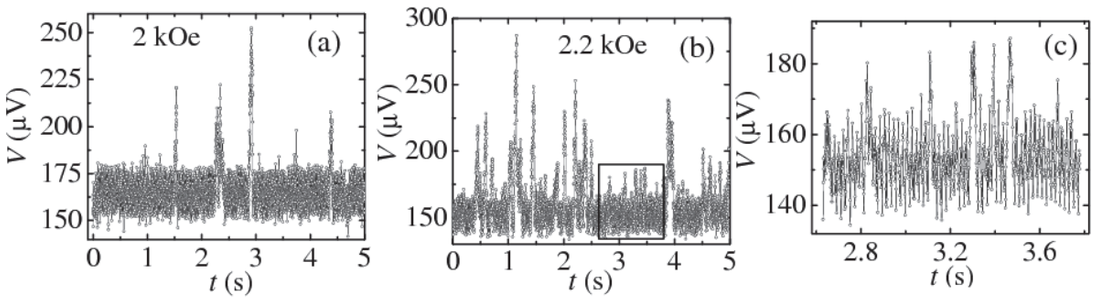

Fig. 17. Panels (a) and (b) show the measured temporal response of the dc voltage (V(t)) at 6 K in the plastic flux-flow regime. Panel (c) is a blow-up of the rectangular region marked in (b). [Mohan et al. 2009a; Mohan 2009b]

One can capture the time resolved voltages (V(t)) in smaller time intervals of 1.25 ms (as against the 35 ms interval in the earlier data) using the data storage buffer of the ADC in a lock-in amplifier. At a higher T and deep in the plastic phase, one observe, the development of an interesting fluctuation behaviour in the time domain, viz., that of intermittency (Mohan et al, 2009a). The panels (a) and (b) in Fig.17 show the measured V(T) data at 6 K in the plastic regime with H=2 kOe and H=2.2 kOe (see phase diagram in the inset of Fig.10). At 2 kOe, one observes nearly-periodic fluctuations about a mean level 160 μV. But, these V fluctuations are interrupted by large, sudden voltage bursts. On entering deeper into the plastic regime, i.e. at 2.2 kOe, these chaotic voltage bursts become much more prominent (see Fig.17(b)). The intermittent large V (equivalent to v) bursts are almost twice as large as the mean V level. In terms of the vortex velocity (v=V/Bd), the mean velocity level at 6 K and 30 mA, is 750 mm/sec whereas during the intermittent bursts the voltage shoots up to a

maximum v ~ 1500 mm/sec. Such bursts are followed by time intervals, when the fluctuations are nearly periodic, as can be clearly seen in panel (c) of Fig.17. Here, it is useful to mention that from simulations studies Olive and Soret (2006, 2008) have proposed that in the plastic regime of flow the vortex motion within the channels periodically synchronizes with the fluctuating vortices trapped in the pinned islands leading to periodic fluctuations. This periodic regime can become unstable and give way to a chaotic burst, with large velocity fluctuations. The intermittent velocity bursts indicate the onset of disordered trajectories of the moving vortices, which is symptomatic of the onset of chaotic motion of vortices. Apart from observing intermittency features in the plastic flow regime (Fig.17) at 6 K there are indirect evidences at 14 kOe at 4.5 K close to $T_c(H)$ (see Fig.13(a)) and Fig.15(a), which indicate the onset of chaotic behavior at these T, H. Perhaps onset of such intermittant velocity bursts appear closer to a regime where thermal fluctuations also begin to play a significant role in the behavior of the vortices in the driven state especially after the onset of plastic flow.

5. Epilogue and future directions

The nonlinear response deep within the driven elastic medium is presumably related to a possible transformation into a heterogenous vortex configuration observed deep within the elastic phase (Mohan et al, 2007). Complex nonlinear systems under certain conditions can produce slow spontaneous organization in its dynamics. Under the influence of a sufficient driving force, the system can exhibit coherent dynamics, with well-defined one or more frequencies (Ganapati & Sood 2006; Ganapati et al., 2008). The evolution of fluctuations, such as those illustrated in Figures 12, 13 and 14, can be viewed as the complex behavior of a nonlinear driven vortex state with multiple attractors (stable cycles). The appearance of stable cycles are characteristic of a particular phase of the driven vortex state. Underlying phase transformations in the driven vortex state induce the system to fluctuate between different stable cycles, leading to a typical spectrum of fluctuations discussed in Figs. 12, 13 and 14. The above nature may lead to extreme sensitivity of the driven vortex system to the low amplitude perturbations, as is shown in Fig.15. We believe that the fluctuations with characteristic frequencies with the nonlinear response discussed above are indicative of phase transformations in the driven vortex state. Figures 15 and 16 have shown that the behavior the characteristic low frequencies f_0 and f'_0 are distinct and cannot be completely attributed to irregular edge related effects of the superconductor. Infact f_0 can be attributed to the due to the elastic fraction of the vortices, where its response is found to be maximum in Figs.12-16, while the 2 Hz represents to disordered fraction in the driven vortex state.

To summarise, we have dwelled the nature of transformations deep in the quasi static elastic vortex state. As the vortex state is driven in the steady state, exploration of vortex-velocity fluctuations in the time domain have uncovered signatures of complex nonlinear dynamics even deep in the elastic driven vortex state prior to the onset of plastic flow. These pertain to new regimes of coherent driven dynamics in the elastic phase with distinct frequencies of fluctuations. These regimes are a precursor to chaotic fluctuations, which can germinate deep in the plastic regime. In ongoing experiments pertaining to more detailed time series measurements on systems other than $NbSe_2$, novel interesting signatures of critical behaviour at dynamical phase transition in driven mode of plastically deformed vortex matter have recently been identified (Banerjee et al, 2011, unpublished).

6. Acknowledgements

We first acknowledge Prof. A.K. Sood of I.I.Sc., Bangalore for sharing his insights on non-linear response in soft condensed matter and motivating our recent investigations in vortex state studies. The author acknowledge Prof. Shobo Bhattacharya and Prof. Eli Zeldov for collaborative works in the past. A.K. Grover thanks C.V. Tomy, Geetha Balakrishnan, M.J. Higgins and P.L. Gammel for the crystals of 2H-$NbSe_2$ for vortex state studies at TIFR. We thank Ulhas Vaidya for his help during experiments at TIFR. Satyajit S. Banerjee (S. S. Banerjee) acknowledges funding from DST, CSIR, DST Indo-Spain S &T forum, IIT Kanpur.

7. References

Angurel, L. A., Amin, F., Polichetti, M., Aarts, J. & Kes, P. H. (1997). Dimensionality of Collective Pinning in 2*H*-$NbSe_2$ Single Crystals. *Physical Review B* Vol. 56, No. 6, pp. 3425-3432

Banerjee, S. S., Patil, N. G., Saha, S., Ramakrishnan, S., Grover, A. K., Bhattacharya, S., Ravikumar, G., Mishra, P. K., Chandrasekhar T. V. Rao, Sahni, V. C., Higgins, M. J., Yamamoto, E., Haga, Y., Hedo, M., Inada, Y. & Onuki, Y. (1998). Anomalous Peak Effect in $CeRu_2$ and 2*H*-$NbSe_2$: Fracturing of a Flux Line Lattice. *Physical Review B* Vol. 58, No. 2, pp. 995-999

Banerjee, S. S., Patil, N. G., Ramakrishnan, S., Grover, A. K., Bhattacharya, S., Ravikumar, G., Mishra, P. K., Rao, T. V. C., Sahni, V. C. & Higgins, M. J. (1999a). Metastability and Switching in the Vortex State of 2*H*-$NbSe_2$. *Applied Physics Letters* Vol. 74, No. 1, pp. 126-128

Banerjee, S. S., Patil, N. G., Ramakrishnan, S., Grover, A. K., Bhattacharya, S., Ravikumar, G., Mishra, P. K., Rao, T. V. C., Sahni, V. C., Higgins, M. J., Tomy, C. V., Balakrishnan, G. & Mck Paul, D. (1999b). Disorder, Metastability, and History Dependence in Transformations of a Vortex Lattice. *Physical Review B* Vol. 59, No. 9, pp. 6043-6046

Banerjee, S. S., Ramakrishnan, S., Grover, A. K., Ravikumar, G., Mishra, P. K., Sahni, V. C., Tomy, C. V., Balakrishnan, G., Paul, D. Mck., Gammel, P. L., Bishop, D. J., Bucher, E., Higgins, M. J. & Bhattacharya, S. (2000a). Peak Effect, Plateau Effect, and Fishtail Anomaly: The Reentrant Amorphization of Vortex Matter in 2*H*-$NbSe_2$. *Physical Review B* Vol. 62, No. 17, pp. 11838-11845

Banerjee, S. S., (2000b). In: Vortex State Studies In Superconductors. *Thesis. Tata Institute of Fundamental Research, Mumbai – 400005. University of Mumbai. India*

Banerjee, S. S., Grover, A. K., Higgins, M. J., Menon, Gautam I., Mishra, P. K. , Pal, D., Ramakrishnan, S., Chandrasekhar Rao, T.V., Ravikumar, G., Sahni, V. C., Sarkar S. and Tomy C.V. (2001) Disordered type-II superconductors: a universal phase diagram for low-Tc systems, Physica C Vol 355, pp. 39 – 50.

Bean, C. P. (1962). Magnetization of Hard Superconductors. *Physical Review Letters* Vol. 8, No. 6, pp. 250-253

Bean, C. P. (1964). Magnetization of High-Field Superconductors. *Reviews of Modern Physics* Vol. 36, No. 1, pp. 31-39

Berlincourt, T. G., Hake, R. R. & Leslie, D. H. (1961). Superconductivity at High Magnetic Fields and Current Densities in Some Nb-Zr Alloys. *Physical Review Letters* Vol. 6, No. 12, pp. 671 -674

Bhattacharya, S. & Higgins, M. J. (1993). Dynamics of a Disordered Flux Line Lattice. *Physical Review Letters* Vol. 70, No. 17, pp. 2617-2620

Blatter G., Feigel'man, M. V., Geshkenbein, V. B., Larkin, A. I. & Vinokur, V. M. (1994). Vortices in High-Temperature Superconductors. *Reviews of Modern Physics* Vol. 66, No. 4, pp. 1125-1388

Blatter, G., Geshkenbein, V. B. & Koopmann, J. A. G. (2004). Weak to Strong Pinning Crossover. *Physical Review Letters* Vol. 92, No. 6, pp. 067009(1)-067009(4)

Le Doussal, P. & Giamarchi, T. (1998). Moving Glass Theory of Driven Lattices with Disorder. *Physical Review B* Vol. 57, No. 18, pp. 11356-11403

Duarte, A., Righi, E. F., Bolle, C. A., Cruz, F. de la, Gammel, P. L., Oglesby, C. S., Bucher, E., Batlogg, B. & Bishop, D. J. (1996). Dynamically Induced Disorder in the Vortex Lattice of 2*H*-$NbSe_2$. *Physical Review B* Vol. 53, No. 17, pp. 11336-11339

Faleski, M. C., Marchetti, M.C. & Middleton, A. A. (1996). Vortex Dynamics and Defects in Simulated Flux Flow. *Physical Review B* Vol. 54, No. 17, pp. 12427-12436

Fiory, A. T. (1971). Quantum Interference Effects of a Moving Vortex Lattice in Al Films. *Physical Review Letters* Vol. 27, No. 8, pp. 501-503

Fisher, M. P. A. (1989). Vortex Glass Superconductivity: A Possible New Phase in Bulk High-T_c Oxides. *Physical Review Letters* Vol. 62, No. 12, pp. 1415-1418

Fisher, D. S., Fisher, M. P. A. & Huse, D. A. (1990). Thermal Fluctuations, Quenched Disorder, Phase Transitions, and Transport in Type-II Superconductors. *Physical Review B* Vol. 43, No. 1, pp. 130-159

Fleming, R. M. & Grimes, C. C. (1979). Sliding-Mode Conductivity in $NbSe_3$: Observation of a Threshold Electric Field and Conduction Noise. *Physical Review Letters* Vol. 42, No. 21, pp. 1423-1426

Gammel, P. L., Yaron, U., Ramirez, A. P., Bishop, D. J., Chang, A. M., Ruel, R., Pfeiffer, L. N., Bucher, E., D'Anna, G., Huse, D. A., Mortensen, K., Eskildsen, M. R. & Kes, P. H. (1998). Structure and Correlations of the Flux Line Lattice in Crystalline Nb Through the Peak Effect. *Physical Review Letters* Vol. 80, No. 4, pp. 833-836

Ganapathy, R. & Sood, A. K. (2006). Intermittent Route to Rheochaos in Wormlike Micelles with Flow-Concentration Coupling. *Physical Review Letters* Vol. 96, No. 10, pp. 108301(1)-108301(4)

Ganapathy, R., Mazumdar, S. & Sood, A. K. (2008). Spatiotemporal Nematodynamics in Wormlike Micelles Enroute to Rheochaos. *Physical Review E* Vol. 78, No. 2, pp. 021504(1)- 021504(6)

Ghosh, K., Ramakrishnan, S., Grover, A. K., Menon, G. I., Chandra, G., Rao, T. V. C., Ravikumar, G., Mishra, P. K., Sahni, V. C., Tomy, C. V., Balakrishnan, G., Mck Paul, D. & Bhattacharya, S. (1996). Reentrant Peak Effect and Melting of a Flux Line Lattice in 2H-$NbSe_2$. *Physical Review Letters* Vol. 76, No. 24, pp. 4600-4603

Giamarchi T. & Le Doussal, P. (1995). Elastic Theory of Flux Lattices in the Presence of Weak Disorder. *Physical Review B* Vol. 52, No. 2, pp. 1242-1270

Giamarchi, T. & Le Doussal, P. (1996). Moving Glass Phase of Driven Lattices. *Physical Review Letters* Vol. 76, No. 18, pp. 3408-3411

Giamarchi, T. & Bhattacharya, S. (2002). Vortex Phases, In: *High Magnetic Fields: Applications in Condensed Matter Physics and Spectroscopy*, C. Berthier, L. P. Levy and G. Martinez (Eds.), *Springer*, 314-360, ISBN: 978-3-540-43979-0

Ghosh, K., Ramakrishnan, S., Grover, A. K., Menon, G. I., Chandra, Girish, Chandrasekhar Rao, T. V., Ravikumar, G., Mishra, P. K., Sahni, V. C., Tomy, C. V., Balakrishnan, G.,

Mck Paul, D., Bhattacharya, S. (1996) Reentrant peak effect and melting of flux line lattice in 2H-$NbSe_2$. *Physical Review Letters* Vol. 76, pp. 4600 – 4603.

Gordeev, S. N., de Groot, P. A. J., Ousenna, M., Volkozub, A. V., Pinfold, S., Langan, R., Gagnon, R. & Taillefer, L. (1997). Current-Induced Organization of Vortex Matter in Type-II Superconductors. *Nature* Vol. 385, pp. 324-326

Harris, J. M., Ong, N. P., Gagnon, R. & Taillefer, L.(1995). Washboard Frequency of the Moving Vortex Lattice in $YBa_2Cu_3O_{6.93}$ Detected by ac-dc Interference. *Physical Review Letters* Vol. 74, No. 18, pp. 3684-3687

Higgins, M. J. & Bhattacharya, S. (1996). Varieties of Dynamics in a Disordered Flux-Line Lattice. *Physica C* Vol. 257, pp. 232-254

Kim, Y. B., Hempstead, C. F. & Strnad, A. R. (1962). Critical Persistent Currents in Hard Superconductors. *Physical Review Letters* Vol. 9, No. 6, pp 306-309

Kokubo, N. , Kadowaki, K. and Takita, K. (2005). Peak Effect and Dynamic Melting of Vortetex matter in $NbSe_2$ Crystals. *Physical Review Letters* Vol. 95, No. 17, pp 177005(1)-177005(4)

Larkin, A. I. & Ovchinnikov, Yu. N. (1979). Pinning in Type II Superconductors. *Journal of Low Temperature Physics*, Vol. 34, No. 3/4, pp 409-428

Larkin, A.I. (1970a). Vliyanie neodnorodnostei na strukturu smeshannogo sostoyaniya sverkhprovodnikov. *Zh. Eksp. Teor.* Fiz, Vol. 58, No. 4, pp. 1466-1470

Larkin, A.I. (1970b). Effect of inhomogeneities on the structure of the mixed state of superconductors, *Sov. Phys. JETP* Vol. 31, No. 4, pp 784

Li, G., Andrei, E. Y. , Xiao, Z. L., Shuk, P. & Greenblatt. M. (2005). Glassy Dynamics in a Moving Vortex Lattice. *J. de Physique IV,* Vol. 131, pp 101-106 (and references therein to their earlier work)

Li, G., Andrei, E. Y., Xiao, Z. L., Shuk, P. & Greenblatt, M. (2006). Onset of Motion and Dynamic Reordering of a Vortex Lattice. *Physical Review Letters* Vol. 96, No. 1, pp 017009(1)-017009(4)

Ling X. S., Park, S. R., McClain, B. A., Choi, S. M., Dender D. C. & Lynn J. W. (2001). Superheating and Supercooling of Vortex Matter in a Nb Single Crystal: Direct Evidence of a Phase Transition at the Peak Effect from Neutron Diffraction. *Physical Review Letters* Vol. 86, No. 4, pp 712-715

Marchevsky, M., Higgins, M. J. & Bhattacharya, S. (2001). Two Coexisting Vortex Phases in the Peak Effect Regime in a Superconductor. *Nature*, Vol. 409, pp 591-594

Marley, A. C., Higgins, M. J. and Bhattacharya, S. (1995). Flux Flow Noise and Dynamical Transitions in a Flux Line Lattice. *Physical Review Letters*, Vol. 74, No. 15, pp 3029-3032

Merithew, R. D., Rabin, M. W., Weissman, M. B., Higgins, M. J. and Bhattacharya, S. (1996). *Physical Review Letters* Vol. 77, No. 15, pp 3197-3199

Mohan, S., Sinha, J., Banerjee, S. S. & Myasoedov, Y., (2007). Instabilities in the vortex matter and the peak effect phenomenon. *Physical Review Letters* Vol. 98, No. 2, pp 027003 (1)-027003(4)

Mohan, S., Sinha, J., Banerjee, S. S., Sood, A. K., Ramakrishnan, S.& Grover, A. K. (2009a). Large Low-Frequency Fluctuations in the Velocity of a Driven Vortex Lattice in a Single Crystal of 2H-$NbSe_2$ Superconductor. *Physical Review Letters* Vol. 103, No. 16, pp 167001(1)-167001(4)

Mohan, S., (2009b). In: Instabilities in the vortex state of type II superconductors. *Thesis. Department of Physics. Indian Intitute of Technology – Kanpur, India*

Natterman, T and Scheidl, S (2000), Vortex - Glass phases in type II superconductors, *Advances in Physics* 1460-6967, 49, 607-705.

Nelson, D. R. (1988). Vortex Entanglement in High *T*c Superconductors. *Physical Review Letters* Vol. 60, No. 19, pp 1973-1976

Nori, F. (1996). Intermittently Flowing River of Magnetic Flux. *Science* Vol. 271, pp 1373-1374

Olive, E. & Soret, J. C. (2006) Chaotic Dynamics of Superconductor Vortices in the Plastic Phase. *Physical Review Letters* Vol. 96, No. 2, pp 027002(1)-027002(4)

Olive, E. & Soret, J. C. (2008). Chaos and Plasticity in Superconductor Vortices: Low-Dimensional Dynamics. *Physical Review B* Vol. 77, No. 14, pp 144514(1)-144514(8)

Pippard A. B, (1969). A Possible Mechanism for the Peak Effect in Type II Superconductors. *Philosophical Magazine* Vol. 19, No. 158, pp 217-220

Paltiel, Y., Fuchs, D. T., Zeldov, E., Myasoedov, Y., Shtrikman, H., Rappaport, M. L. & Andrei, E. Y. (1998). Surface Barrier Dominated Transport in $NbSe_2$, *Physical Review B* Vol. 58, No. 22, R14763-R14766

Paltiel, Y., Zeldov, E., Myasoedov, Y. N., Shtrikman, H., Bhattacharya, S., Higgins, M. J., Xiao, Z. L., Andrei, E. Y., Gammel, P. L. & Bishop, D. J. (2000). Dynamic Instabilities and Memory Effects in Vortex Matter. *Nature*, Vol. 403, pp 398-401

Paltiel, Y., Jung, G., Myasoedov, Y., Rappaport, M. L., Zeldov, E., Higgins, M. J. & Bhattacharya, S. (2002). Dynamic Creation and Annihilation of Metastable Vortex Phase as a Source of Excess Noise. *Europhysics Letters* Vol. 58, No. 1, pp 112-118

Shi, A. C. & Berlinsky, A. J. (1991). Pinning and *I-V* characteristics of a two-dimensional defective flux-line lattice. *Physical Review Letters* Vol. 67, No. 14, pp 1926-1929

Thakur, A. D., Banerjee, S. S., Higgins, M. J., Ramakrishnan, S. and Grover, A. K. (2005) Exploring metastability via third harmonic measurements in single crystals of 2H-$NbSe_2$ showing an anomalous peak effect. *Physical Review B* Vol.72, pp 134524-134529.

Thakur, A. D., Banerjee, S. S., Higgins, M. J., Ramakrishnan, S. and Grover, A. K. (2006) Effect of pinning and driving force on the metastability effects in weakly pinned superconductors and the determination of spinodal line pertaining to order-disorder transition. *Pramana Journal of Physics* Vol. 66, pp. 159 – 177.

Troyanovski, A. M., Aarts, J. & Kes, P.H. (1999). Collective and plastic vortex motion in superconductors at high flux densities, *Nature* Vol. 399, pp 665-668

Troyanovski, A. M., van Hecke, M., Saha, N., Aarts, J. & Kes, P. H. (2002). STM imaging of flux line arrangements in the peak-effect regime. *Physical Review Letters* Vol. 89, No. 14, pp 147006(1)-147006(4)

Xiao, Z. L., Andrei, E. Y. & Higgins, M. J. (1999). Flow Induced Organization and Memory of a Vortex Lattice. *Physical Review Letters* Vol.83, No. 8, pp 1664-1667.

Yaron, U., Gammel, P. L., Huse, D. A., Kleiman, R. N., Oglesby, C. S., Bucher, E., Batlogg, B., Bishop, D. J., Mortensen, K., Clausen, K., Bolle, C. A. & de la Cruz, F. (1994). Neutron Diffraction Studies of Flowing and Pinned Magnetic Flux Line Lattices in $2HNbSe_2$. *Physical Review Letters* Vol. 73, No. 20, pp 2748-2751 (1994)

Zeldov, E., Larkin, A. I., Geshkenbein, V. B., Konczykowski, M., Majer, D., Khaykovich, B., Vinokur, V. M. & Shtrikman, H. (1994). Geometrical Barriers in High-Temperature Superconductors, *Physical Review Letters* Vol. 73, No. 10, pp 1428-1431.

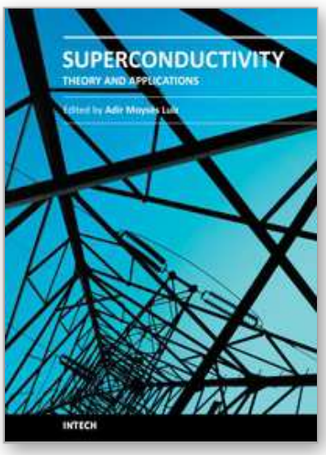

Superconductivity - Theory and Applications
Edited by Dr. Adir Luiz

ISBN 978-953-307-151-0
Hard cover, 346 pages
Publisher InTech
Published online 18, July, 2011
Published in print edition July, 2011

Superconductivity was discovered in 1911 by Kamerlingh Onnes. Since the discovery of an oxide superconductor with critical temperature (Tc) approximately equal to 35 K (by Bednorz and Müller 1986), there are a great number of laboratories all over the world involved in research of superconductors with high Tc values, the so-called â€œHigh-Tc superconductorsâ€. This book contains 15 chapters reporting about interesting research about theoretical and experimental aspects of superconductivity. You will find here a great number of works about theories and properties of High-Tc superconductors (materials with Tc > 30 K). In a few chapters there are also discussions concerning low-Tc superconductors (Tc < 30 K). This book will certainly encourage further experimental and theoretical research in new theories and new superconducting materials.

InTech Europe
University Campus STeP Ri
Slavka Krautzeka 83/A
51000 Rijeka, Croatia
Phone: +385 (51) 770 447
Fax: +385 (51) 686 166
www.intechopen.com

InTech China
Unit 405, Office Block, Hotel Equatorial Shanghai
No.65, Yan An Road (West), Shanghai, 200040, China
中国上海市延安西路65号上海国际贵都大饭店办公楼405单元
Phone: +86-21-62489820
Fax: +86-21-62489821

IntechOpen